NACA RM L53D09

NACA

RESEARCH MEMORANDUM

LOW-SPEED, LARGE-SCALE INVESTIGATION OF AERODYNAMIC CHARACTERISTICS OF A SEMISPAN 49° SWEPTBACK WING WITH A FOWLER FLAP IN COMBINATION WITH A PLAIN FLAP, SLATS, AND FENCES

By Edward F. Whittle, Jr., and Stanley Lipson

Langley Aeronautical Laboratory
Langley Field, Va.

NATIONAL ADVISORY COMMITTEE
FOR AERONAUTICS

WASHINGTON

June 5, 1953

NATIONAL ADVISORY COMMITTEE FOR AERONAUTICS

RESEARCH MEMORANDUM

LOW-SPEED, LARGE-SCALE INVESTIGATION OF AERODYNAMIC CHARACTERISTICS OF A SEMISPAN 49° SWEPTBACK WING WITH A FOWLER FLAP IN COMBINATION WITH A PLAIN FLAP, SLATS, AND FENCES

By Edward F. Whittle, Jr., and Stanley Lipson

SUMMARY

An investigation has been conducted in the Langley full-scale tunnel to determine the effects of a Fowler type slotted flap on the aerodynamic characteristics of a semispan 49.1° sweptback wing having NACA 65A006 airfoil sections streamwise, an aspect ratio of 3.78, and a taper ratio of 0.59. Various slat and fence arrangements were tested in combination with the Fowler flap. The effect of longitudinal and vertical location of the Fowler flap was investigated over a limited range of positions.

In addition, tests were made of a configuration having the Fowler flap located near the trailing edge of a plain flap. When the flaps were deflected, this arrangement tended to produce a double-cambered surface at the rear portion of the wing.

The tests were conducted at Reynolds numbers of 6.1×10^6 and 4.4×10^6 with corresponding Mach numbers of 0.10 and 0.07, respectively.

INTRODUCTION

As part of a general investigation, at large scale, of means of improving the low-speed static longitudinal aerodynamic characteristics of high-speed wing plan forms, tests have been conducted in the Langley full-scale tunnel on a 49.1° sweptback wing equipped with various high-lift and stall-control devices. The wing had an aspect ratio of 3.78, a taper ratio of 0.59, and NACA 65A006 airfoil sections parallel to the plane of symmetry. References 1 and 2 present the results of pressure and force measurements made with various slat, plain trailing-edge flap, and fence arrangements.

This paper presents the results of force tests made, with the main effort directed toward increased lift, on the semispan sweptback wing equipped with a 0.47-semispan Fowler type slotted flap located at several longitudinal and vertical positions. The effect of various slat and fence arrangements on the characteristics of the flapped wing was also investigated. In addition, tests were made of a configuration having the Fowler flap located near the trailing edge of a deflected plain flap.

The tests were made at Reynolds numbers of 6.1×10^6 and 4.4×10^6, with corresponding Mach numbers of 0.10 and 0.67, respectively.

COEFFICIENTS AND SYMBOLS

The data are referred to the wind axes with the origin at the quarter-chord point of the mean aerodynamic chord. The data have been reduced to standard NACA nondimensional coefficients which, together with the symbols, are defined as follows:

C_L lift coefficient, $2L/q_oS$

$C_{L_{\alpha=0}}$ lift coefficient at 0° angle of attack

$\Delta C_{L_{\alpha=0}}$ value of $C_{L_{\alpha=0}}$ for any configuration minus value of $C_{L_{\alpha=0}}$ for basic wing

$C_{L_{max}}$ maximum lift coefficient

$\Delta C_{L_{max}}$ value of $C_{L_{max}}$ for any configuration minus value of $C_{L_{max}}$ for basic wing

C_D drag coefficient, $\dfrac{2 \times \text{Model drag}}{q_oS}$

C_m pitching-moment coefficient about quarter-chord point of mean aerodynamic chord, $\dfrac{2 \times \text{Model pitching moment}}{q_oS\bar{c}}$

b twice model span, ft

c local wing chord measured parallel to plane of symmetry, ft

c'	local wing chord measured perpendicular to center line of a corresponding unswept wing, ft
c'_f	local trailing-edge-flap chord measured perpendicular to 0.50c' line, ft
c'_s	local slat chord measured perpendicular to 0.50c' line, ft
$\bar{c}$	mean aerodynamic chord, $\frac{2}{S}\int_0^{b/2} c^2 dy$, ft
h	distance from wing leading edge to hinge line of Fowler flap, measured perpendicular to 0.50c' line, ft
L	model lift, lb
M	bending moment at wing root, ft-lb
v	perpendicular distance from plain-flap chord plane to hinge line of Fowler flap, ft
q_o	free-stream dynamic pressure, $\frac{\rho V^2}{2}$, lb/sq ft
R	Reynolds number, $\rho V\bar{c}/\mu$
S	twice model wing area, sq ft
V	free-stream velocity, ft/sec
y	spanwise coordinate perpendicular to plane of symmetry, ft
$(c.p.)_y$	spanwise location of wing center of pressure, $M/L \frac{b}{2}$
α	angle of attack, deg
δ_{pf}	plain-flap deflection measured relative to wing chord line in a plane perpendicular to 0.50c' line, deg
δ_{ff}	Fowler flap deflection measured relative to chord line of plain flap in a plane perpendicular to 0.50c' line, deg
$\delta_{ff'}$	Fowler flap deflection measured relative to wing chord line in a plane perpendicular to 0.50c' line, $\delta_{ff} + \delta_{pf}$, deg

ρ mass density of air, slugs/cu ft

μ coefficient of viscosity, slugs/ft-sec

MODEL

The geometric characteristics and principal dimensions of the semispan wing are given in figure 1. Details of the high-lift and stall-control devices (plain flap, Fowler flap, slat, and fences) together with section views of the various combinations tested are shown in figure 2. The semispan wing is shown mounted on a reflection plane in the Langley full-scale tunnel in figure 3. A description of the reflection plane is presented in reference 3. The wing has 49.1° of sweepback at the leading edge, an aspect ratio of 3.78, a taper ratio of 0.59, and no geometric twist or dihedral. The airfoil sections parallel to the plane of symmetry are NACA 65A006 sections. The wing tip is half of a body of revolution based on the same airfoil section ordinates.

The high-lift and stall-control devices used were: a 0.25c' plain flap having a span of 0.469b/2; a 0.20c' Fowler flap having a span of 0.469b/2; 0.15c' leading-edge slats of various lengths; and various combinations of chordwise fences, having a height of 0.06c, installed at various spanwise stations. (See table I.) The fences were made of 1/4-inch plywood and were mounted parallel to the plane of symmetry. For all configurations on which the nose of the fences intersected the slat, and for one case where the spanwise location of a fence practically coincided with the inboard end of the slat, the fences were cut off at 0.05c (see fig. 2(b)). The nose and upper surface of the slat had the airfoil ordinates of the wing but the slat was not an integral part of the wing and was mounted directly on the unmodified leading edge of the basic wing with the slat brackets alined normal to the wing leading edge. The minimum chordwise clearance between the slat and wing and the distance of the slat nose ahead of the wing were selected from the slat-positioning results for two-dimensional flow (ref. 4). Further details of the slat arrangement may be obtained from reference 1.

The Fowler flap was constructed of wood and had a 15-percent-thick symmetrical airfoil section whose ordinates were such as to permit its retraction within the plain flap. The plain flap was made of steel plate and was contoured so as to duplicate the flap employed in the tests of reference 2. Except for one test, whenever the Fowler flap was deflected the undersurface of the plain flap was removed (see fig. 2(a)) in order to simulate more realistically a production configuration.

The Fowler flap was manually positioned and deflected, and was rigidly attached to the plain flap by means of steel brackets (fig. 3(b)). The plain flap was automatically deflected through the use of two electrically powered actuators installed on the lower surface of the wing inside of streamlined fairings (fig. 3(b)). With the Fowler flap installed, deflection of the plain flap produced a double-cambered surface at the rear of the wing (fig. 2(b)).

TESTS AND CORRECTIONS

The model configurations tested are detailed in table I. Force data (lift, drag, pitching moment, and bending moment) were obtained through an angle-of-attack range from about -4° to 32° and at Reynolds numbers of 4.4×10^6 and 6.1×10^6 with corresponding Mach numbers of 0.07 and 0.10, respectively. With the fences installed it was necessary to conduct the tests at a Reynolds number of 4.4×10^6 because the fences tended to vibrate in the high lift-coefficient range at the higher tunnel speed corresponding to a Reynolds number of 6.1×10^6.

The data have been corrected for airstream misalinement, blocking effects, and jet-boundary effects. As discussed in reference 3, the jet-boundary corrections applied to the data were calculated by the procedure outlined in reference 5 from the downwash values for the Langley full-scale tunnel presented in reference 6.

The jet-boundary corrections for the wing are as follows:

$$\Delta\alpha = -0.84C_L$$

$$\Delta C_D = -0.01281C_L^2$$

$$\Delta C_m = -0.00427C_L$$

These values are added to the uncorrected data.

RESULTS

For the present series of tests, the value of $C_{L_{max}}$ for the basic wing was 0.97 (fig. 4) as compared with a value of 1.00 obtained for the same model during the investigation reported in references 1 and 2. The

small difference is probably due to the installation of the two flap-actuator fairings on the lower surface of the wing for the present investigation and to the very small contour changes that may have occurred during the refinishing of the model surface that was required between the present tests and the previous tests of references 1 and 2.

It may be noted that the pitching-moment curve presented in references 1 and 2 for the basic wing configuration is slightly displaced negatively and parallels the pitching-moment data of the present investigation. This discrepancy is due to a flow angularity close to the surface of the reflection plane during the tests of references 1 and 2 which reduced the local angle of attack, and thus the lift, at the wing root. During the present investigation, this angularity was eliminated by the installation of vanes in the tunnel entrance cone.

An index of the test conditions and the configurations tested is given in table I and the results of the tests are presented in figures 4 to 14. A summary of the effect on $\Delta C_{L_{max}}$ and $\Delta C_{L_{\alpha=0}}$ of Fowler flap location, Fowler flap and plain-flap deflections, and Fowler flap deflections tested in combination with various plain-flap deflections is presented in figures 15, 16, and 17, respectively. The effect of slat span on $\Delta C_{L_{max}}$ for the basic wing and flapped wing with fences is illustrated in figure 18.

Although the particular slat-wing combination tested herein may not be an optimum arrangement, because of the use of the unmodified wing leading edge, it is believed that the arrangement is of sufficient aerodynamic efficiency to illustrate the general effects which may be obtained by employing a slat in conjunction with this wing.

In figure 17(a) the results obtained with the Fowler flap deflected 30° in combination with various plain-flap deflections are compared with predicted values which were obtained by simply adding the lift increases produced by the plain flap alone (fig. 16) to the increments due to deflecting the Fowler flap (plain flap neutral, fig. 15).

At this point it is probably appropriate to note again that the Fowler flap angle relative to the wing chord line is altered when the plain flap is deflected, since the Fowler flap is rigidly attached to the plain flap. Thus, in predicting the curves of figure 17(a) by the use of the data in figure 16, as discussed above, the $\Delta C_{L_{max}}$ and $\Delta C_{L_{\alpha=0}}$ values used were for the corresponding values of $\delta_{ff'}$ rather than δ_{ff}.

The effect on $\Delta C_{L_{max}}$ and $\Delta C_{L_{\alpha=0}}$ of varying the plain-flap deflection for $\delta_{ff} = 30^\circ$, $\frac{v}{c'} = 0.95$, and $\frac{h}{c'} = 0.01250$ and for $\delta_{ff} = 45^\circ$, $\frac{v}{c'} = 1.00$, and $\frac{h}{c'} = 0.00625$ is presented in figure 17(b). Inasmuch as the hinge locations were different for the two deflections, this difference must be taken into account before the effect of deflection of the Fowler flap can be determined. Therefore, the data for $\delta_{ff} = 30^\circ$, at $\frac{v}{c'} = 1.00$ and $\frac{h}{c'} = 0.00625$, were predicted from the data of figure 16 by adding the appropriate values of $\Delta C_{L_{max}}$ and $\Delta C_{L_{\alpha=0}}$ for the corresponding deflections $\delta_{ff'}$ and δ_{pf}. Since the results of figure 4 show only small differences in the aerodynamic characteristics in the range of Reynolds numbers tested, the effect on this comparison (fig. 17(b)) of the difference in the two test Reynolds numbers is probably of no significance.

SUMMARY OF RESULTS

The main effort of this investigation has been directed toward determining the influence on the lift effectiveness of the Fowler flap of such flap-positioning parameters as chordwise location, gap size, and deflection angle. Although no detailed analysis has been made of the results presented, a few of the more significant trends of the lift characteristics which can be readily noted from the data are as follows:

1. For the range of Fowler flap locations tested herein, the more rearward positions produced the greater values of $\Delta C_{L_{max}}$ and $\Delta C_{L_{\alpha=0}}$ (fig. 15(a)).

2. At the larger Fowler flap deflections ($\delta_{ff} = 45^\circ$), gap size has a significant effect on $\Delta C_{L_{\alpha=0}}$ (fig. 15(b)).

3. The lift increments produced by the Fowler flap located near the trailing edge of a plain flap (an arrangement that gives a double-cambered surface at the rear of the wing) can be readily predicted by simply adding the individual lift effects of each flap.

4. When the Fowler flap was deflected, the use of leading-edge stall-control devices of 0.5 semispan or longer produced very significant increases in $\Delta C_{L_{max}}$ (fig. 18).

One of the aims of this investigation, was to obtain satisfactory longitudinal stability at high lift coefficients. The particular combination of sweep, aspect ratio, and airfoil thickness used in the investigation, however, resulted in a severe longitudinal-stability problem. Although none of the test arrangements investigated herein provided satisfactory stability throughout the lift range, several of the fence and slat configurations tested increased the value of the lift coefficient at which the flapped wing first exhibited sudden longitudinal instability and, consequently, resulted in usable lift coefficients through a larger angle-of-attack range. It is probable that for the wing investigated, as was the case for a wing of similar sweep but higher aspect ratio (ref. 7), satisfactory longitudinal stability can be obtained from certain limited combinations of leading-edge-slat and trailing-edge-flap spans.

Langley Aeronautical Laboratory,
National Advisory Committee for Aeronautics,
Langley Field, Va.

REFERENCES

1. Lipson, Stanley, and Barnett, U. Reed, Jr.: Force and Pressure Investigation at Large Scale of a 49° Sweptback Semispan Wing Having NACA 65A006 Sections and Equipped With Various Slat Arrangements. NACA RM L51K26, 1952.

2. Barnett, U. Reed, Jr., and Lipson, Stanley: Effects of Several High-Lift and Stall-Control Devices on the Aerodynamic Characteristics of a Semispan 49° Sweptback Wing. NACA RM L52D17a, 1952.

3. Lipson, Stanley, and Barnett, U. Reed, Jr.: Comparison of Semispan and Full-Span Tests of a 47.5° Sweptback Wing With Symmetrical Circular-Arc Sections and Having Drooped-Nose Flaps, Trailing-Edge Flaps, and Ailerons. NACA RM L51H15, 1951.

4. Gottlieb, Stanley M.: Two-Dimensional Wind-Tunnel Investigation of Two NACA 6-Series Airfoils With Leading-Edge Slats. NACA RM L8K22, 1949.

5. Sivells, James C., and Salmi, Rachel M.: Jet-Boundary Corrections for Complete and Semispan Swept Wings in Closed Circular Wind Tunnels. NACA TN 2454, 1951.

6. Katzoff, S., and Hannah, Margery E.: Calculation of Tunnel-Induced Upwash Velocities for Swept and Yawed Wings. NACA TN 1748, 1948.

7. Salmi, Reino J.: Effects of Leading-Edge Devices and Trailing-Edge Flaps on Longitudinal Characteristics of Two 47.7° Sweptback Wings of Aspect Ratios 5.1 and 6.0 at a Reynolds Number of 6.0×10^6. NACA RM L50F20, 1950.

TABLE I.- INDEX OF TEST CONDITIONS AND CONFIGURATIONS

$R \times 10^{-6}$	Fowler flap position			δ_{pf}	Remarks	Figure number
	h/c'	v/c'	δ_{ff}			
4.4	Fowler flap off			0	Basic wing	4
6.1						
6.1	Fowler flap off			0		5
				10		
				20		
				30		
6.1	Fowler flap off			0	Basic wing	6
	0.90	0.00625	30	0		
	.95	.01250				
	1.00	.02500				
		.01250				
		.00625				
6.1	Fowler flap off			0	Basic wing	7
	.90	.00625	45	0		
	.95	.01250				
	1.00	.02500				
		.01250				
		.00625				
6.1	Fowler flap off			0	Basic wing	8
	.95	.01250	30	0		
				10		
				15		
				20		
				30		
			45	0		
6.1	Fowler flap off			0	Basic wing	9
	1.00	.00625	30	0		
			35			
			40			
			45			
			30	30		
6.1	Fowler flap off			0	Basic wing	10
	1.00	.00625	45	0		
				0	Plain flap undersurface faired and sealed	
4.4				0		
4.4	Fowler flap off			0	Basic wing	11
	1.00	.00625	45	0		
				5		
				10		
				15		

TABLE I.- INDEX OF TEST CONDITIONS AND CONFIGURATIONS - Concluded

$R \times 10^{-6}$	Fowler flap position			δ_{pf}	Fence locations, 2y/b from root	Slat span, 2y/b from tip	Remarks (a)	Figure number
	h/c'	v/c'	δ_{ff}					
4.4	Fowler flap off			0	Off	Off	Basic wing	12
	1.00	0.00625	45	0	Off		Full-chord fences	
					0.4, 0.8			
					0.6, 0.8			
					0.4, 0.6, 0.8			
4.4	Fowler flap off			0	Off	Off	Basic wing	13
	1.00	.00625	45	0	0.6, 0.8	0.375	Partial-chord fences at $\frac{2y}{b} = 0.6, 0.8$	
						.375	Partial-chord fences at $\frac{2y}{b} = 0.8$	
						.425	Partial-chord fences at $\frac{2y}{b} = 0.6, 0.8$	
						.500		
						From 0.425 outboard to 1.000 inboard	Full-chord fences	
4.4	Fowler flap off			0	Off	Off	Basic wing	14
	1.00	.00625	45	0	0.2, 0.6, 0.8	.425	Partial-chord fences at $\frac{2y}{b} = 0.6, 0.8$	
						.500		
					0.4, 0.6, 0.8	.500		
						.625	Partial-chord fences at $\frac{2y}{b} = 0.4, 0.6, 0.8$	
						1.000		

[a]Wherever the slat span was of sufficient length to intersect the leading edge of a full-chord fence, the fence was cut to a partial-chord fence. (See fig. 2(b).)

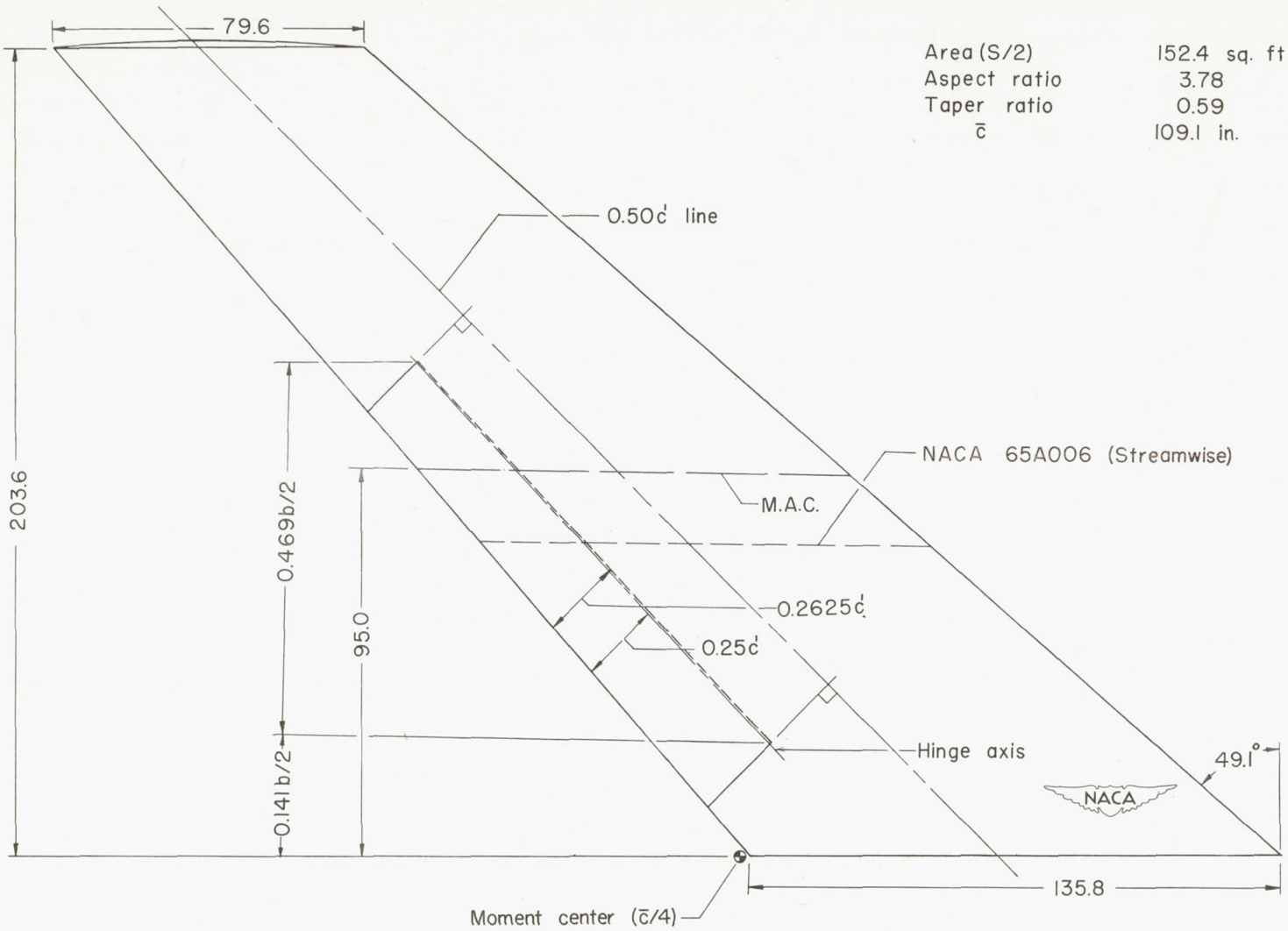

Figure 1.- Plan form of the semispan 49.1° sweptback wing. All dimensions are given in inches unless otherwise noted.

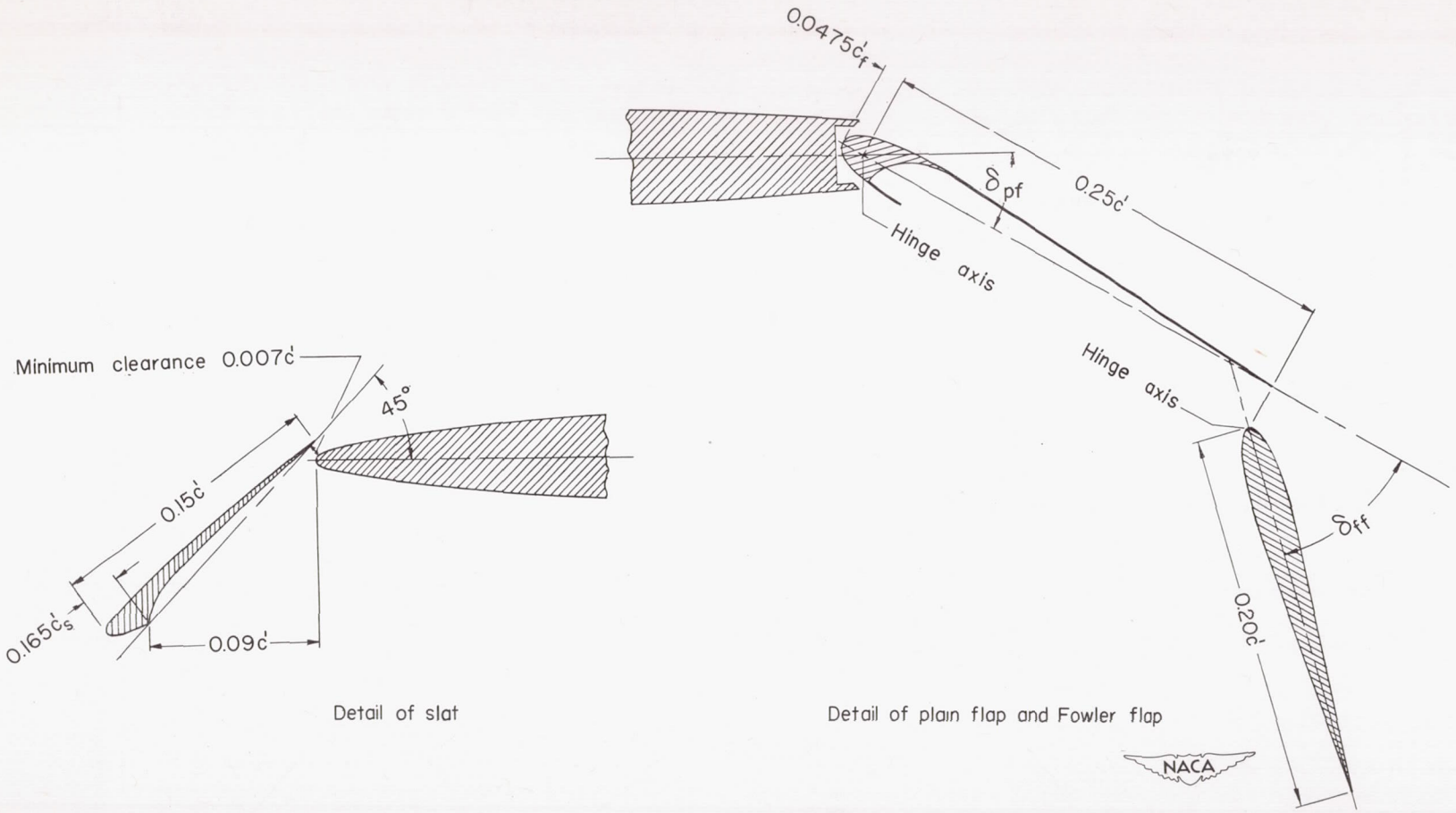

(a) Detail of slat and flaps.

Figure 2.- High-lift and stall-control devices.

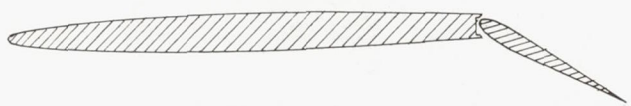

Plain flap deflected

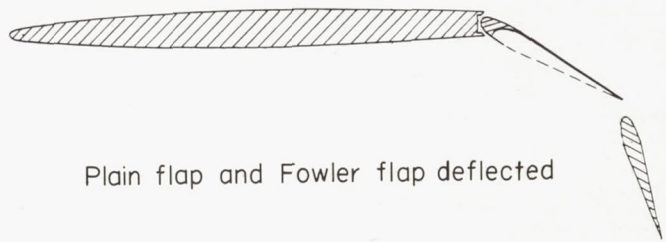

Plain flap and Fowler flap deflected

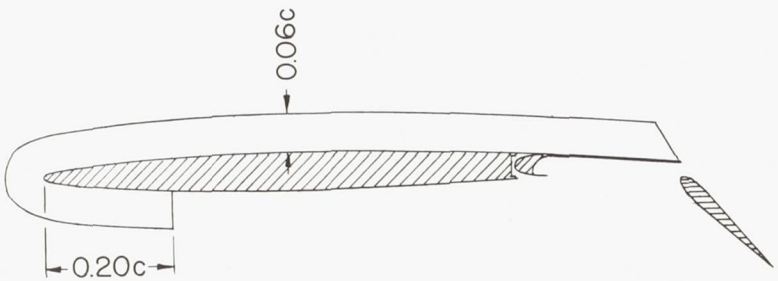

Full-chord fence; Fowler flap deflected

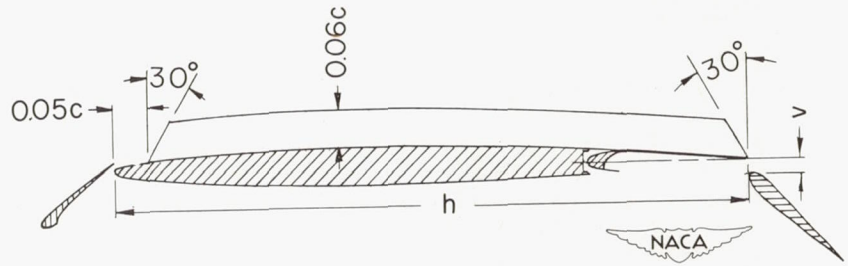

Partial-chord fence; slat deflected; Fowler flap deflected

(b) Configurations tested.

Figure 2.- Concluded.

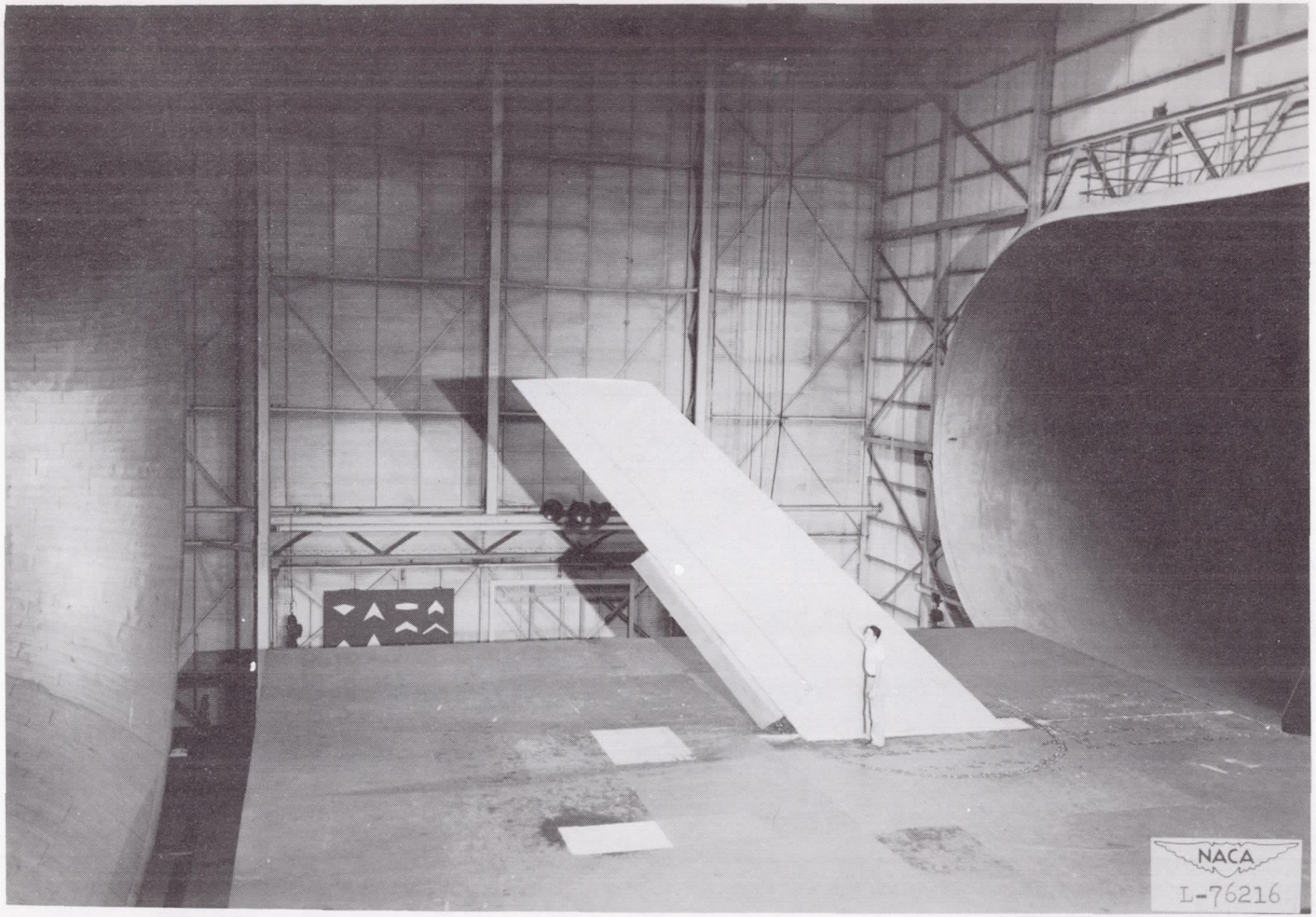

(a) General view of top surface.

Figure 3.- The semispan 49.1° sweptback wing, with Fowler flap installed, mounted in the full-scale tunnel.

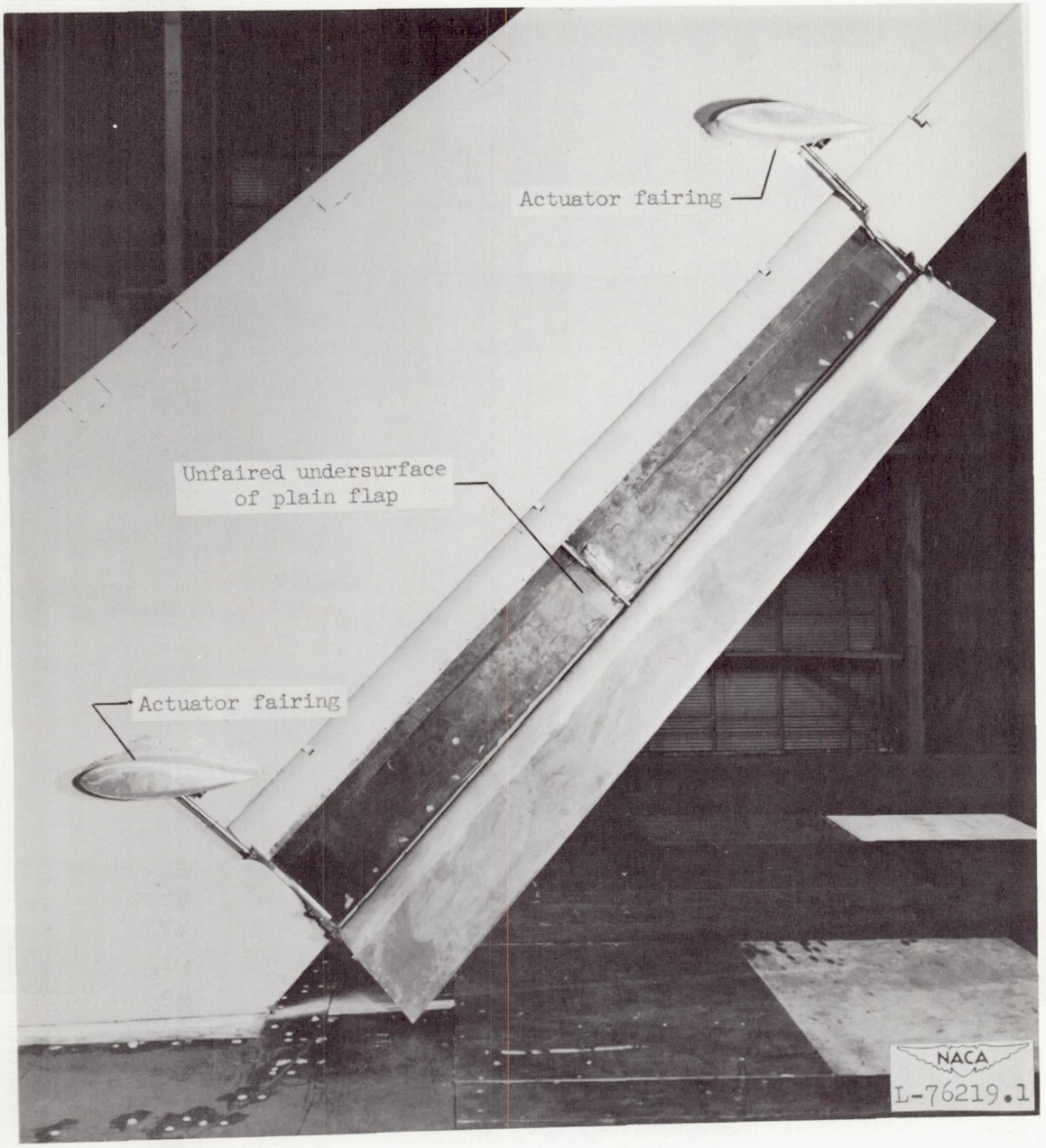

(b) Close-up of undersurface.

Figure 3.- Concluded.

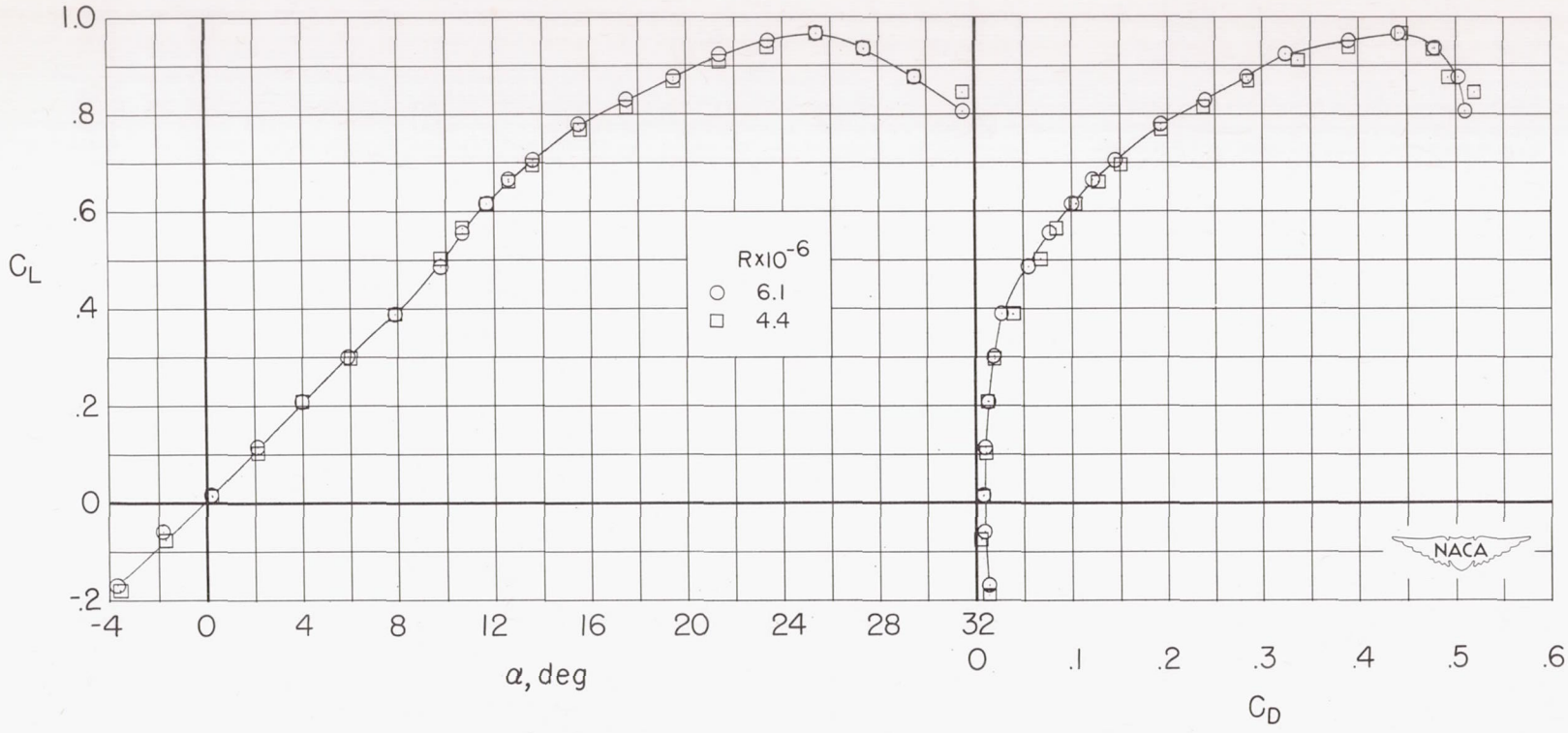

(a) C_L versus α. (b) C_L versus C_D.

Figure 4.- Effect of Reynolds number on aerodynamic characteristics of the semispan 49.1° sweptback wing. Basic wing.

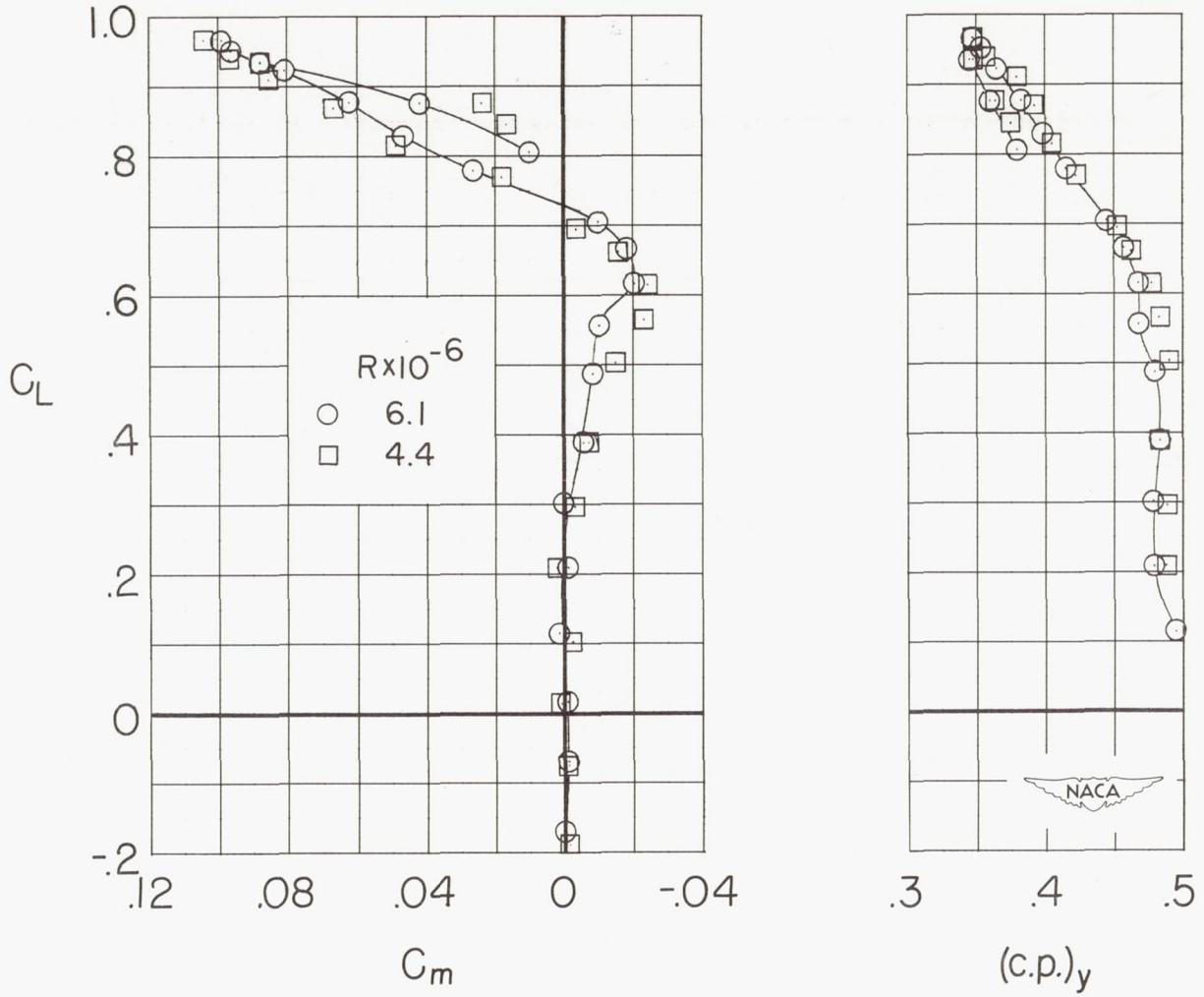

(c) C_L versus C_m.

(d) C_L versus $(c.p.)_y$.

Figure 4.- Concluded.

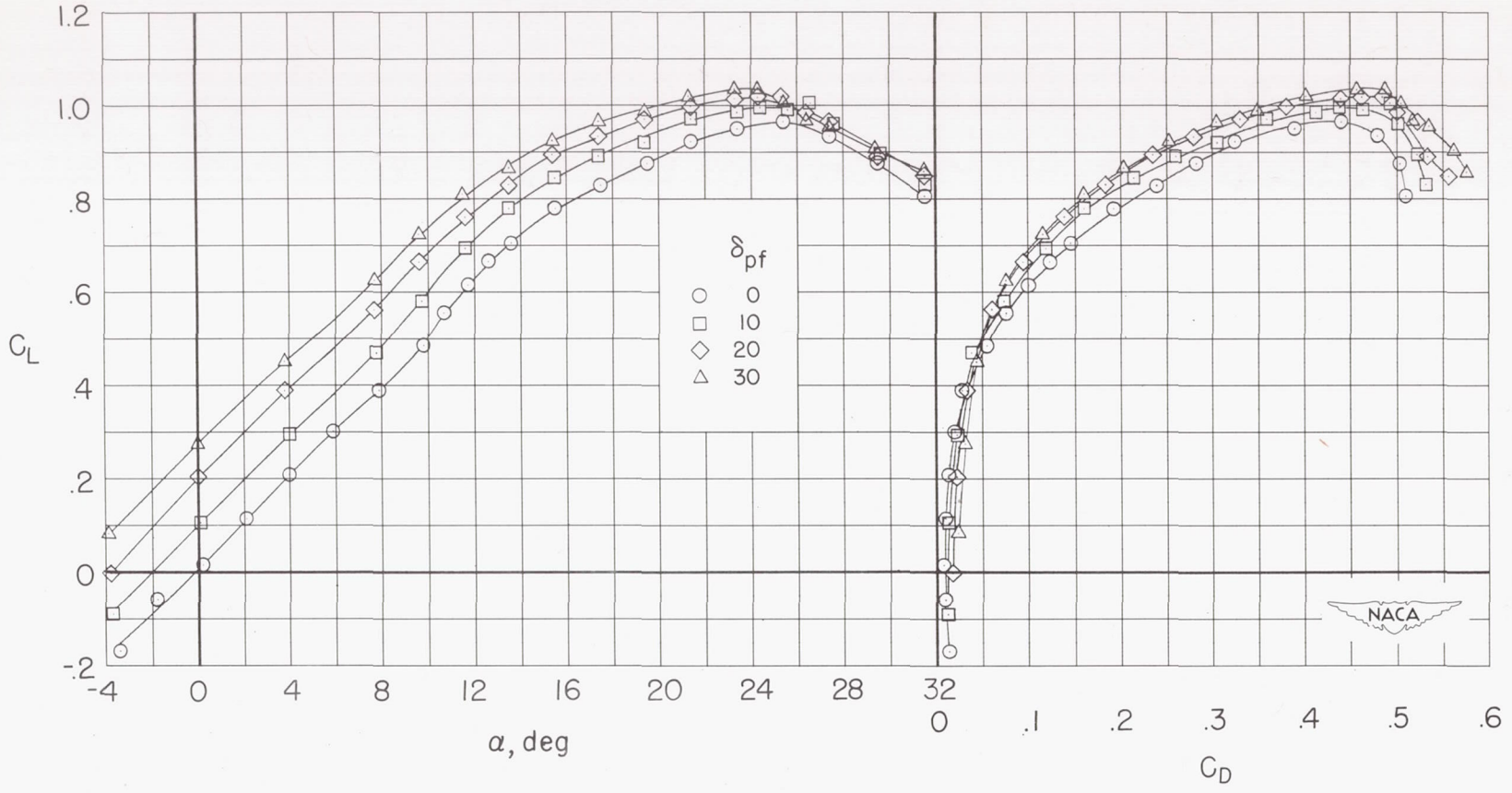

(a) C_L versus α. (b) C_L versus C_D.

Figure 5.- Effect of plain-flap deflection on aerodynamic characteristics of the semispan 49.1° sweptback wing. $R \times 10^{-6} = 6.1$.

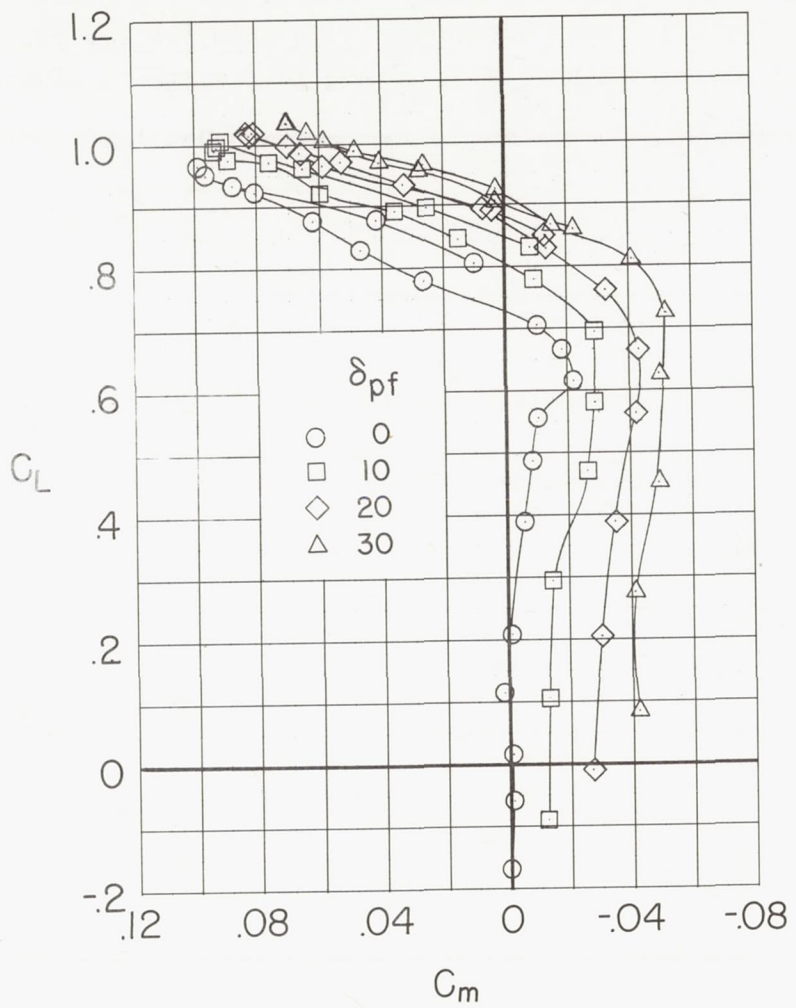

(c) C_L versus C_m.

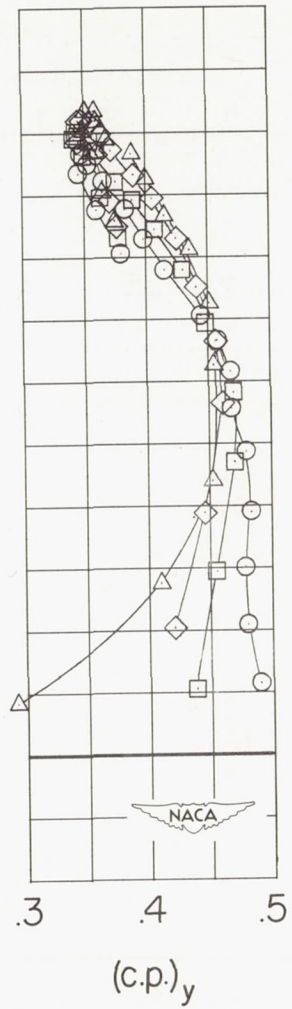

(d) C_L versus $(c.p.)_y$.

Figure 5.- Concluded.

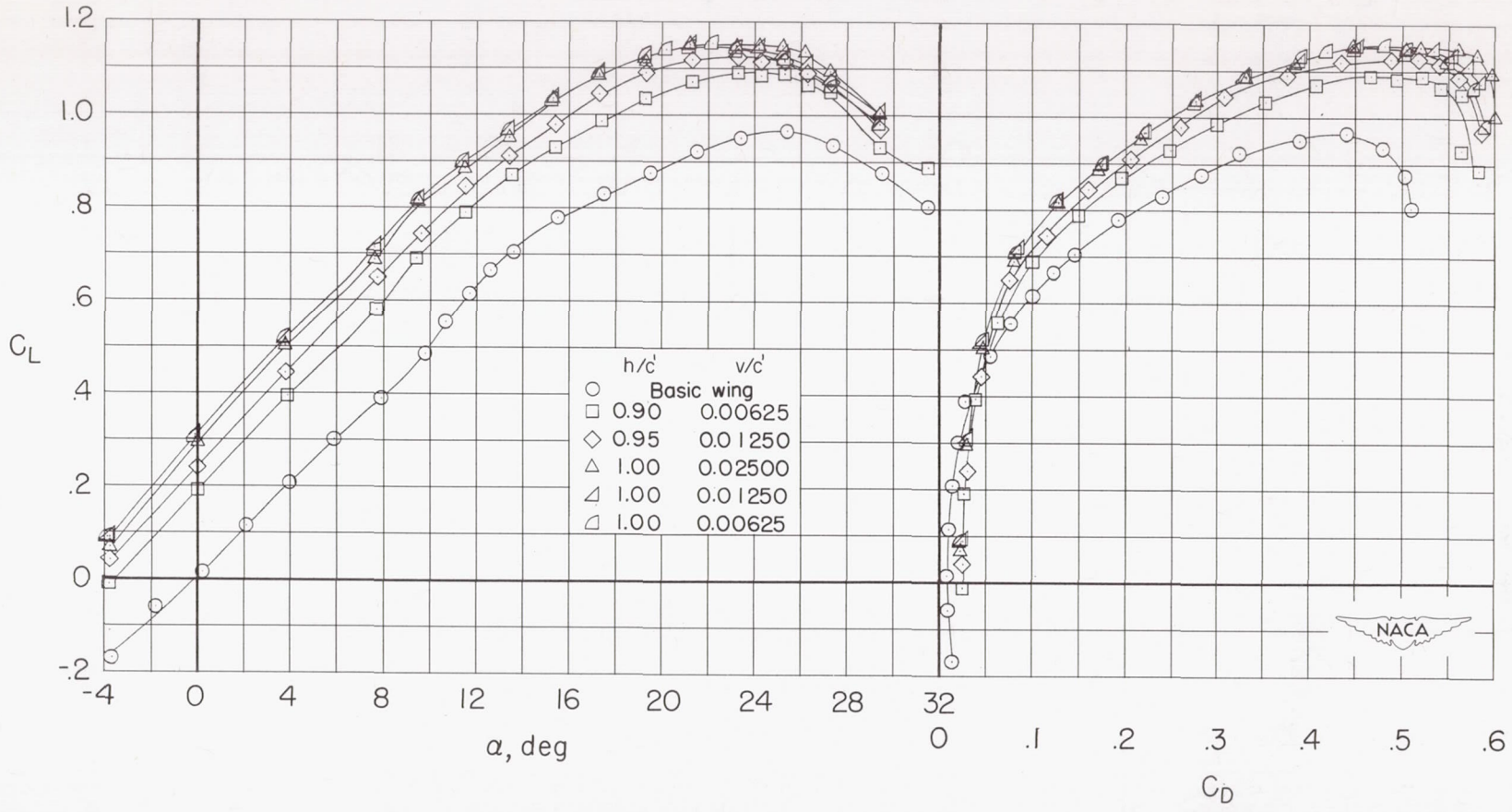

(a) C_L versus α. (b) C_L versus C_D.

Figure 6.- Effect of Fowler flap location on aerodynamic characteristics of the semispan 49.1° sweptback wing. $R \times 10^{-6} = 6.1$; $\delta_{ff} = 30°$; $\delta_{pf} = 0°$.

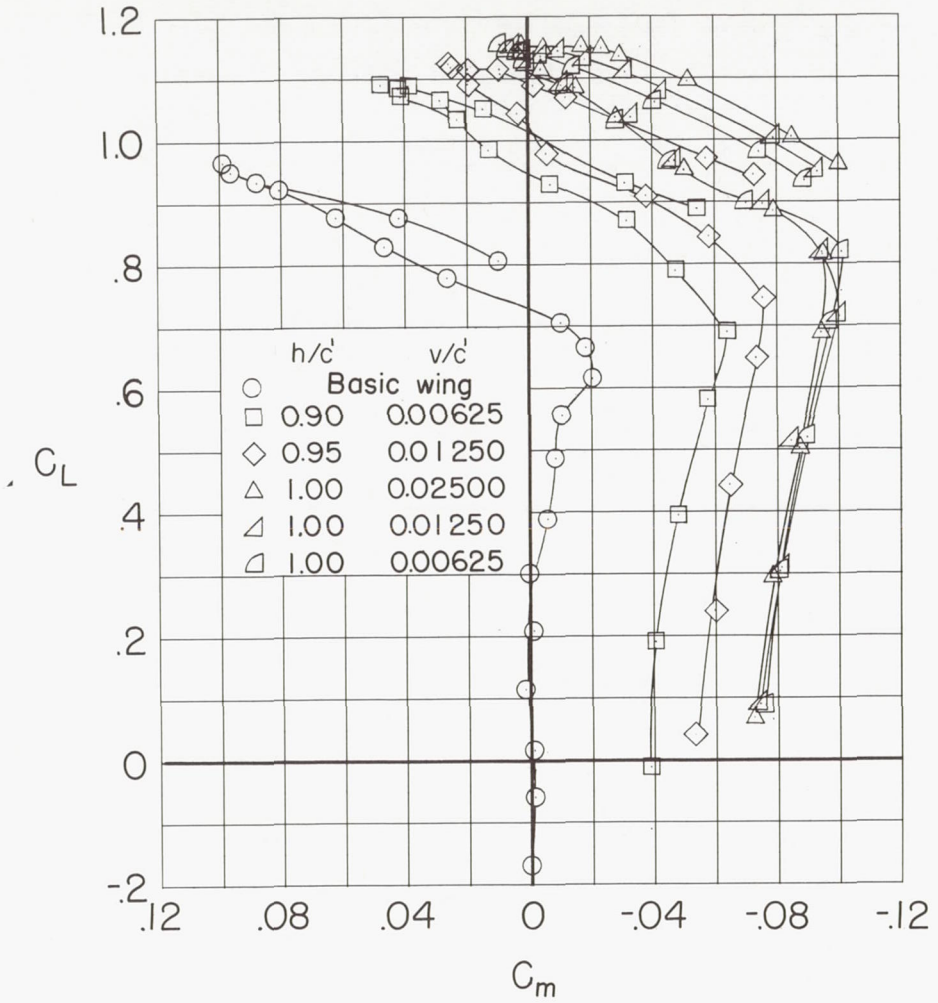

(c) C_L versus C_m.

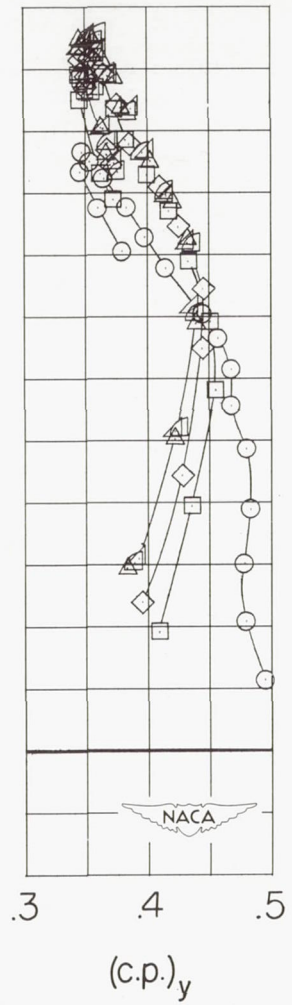

(d) C_L versus $(c.p.)_y$.

Figure 6.- Concluded.

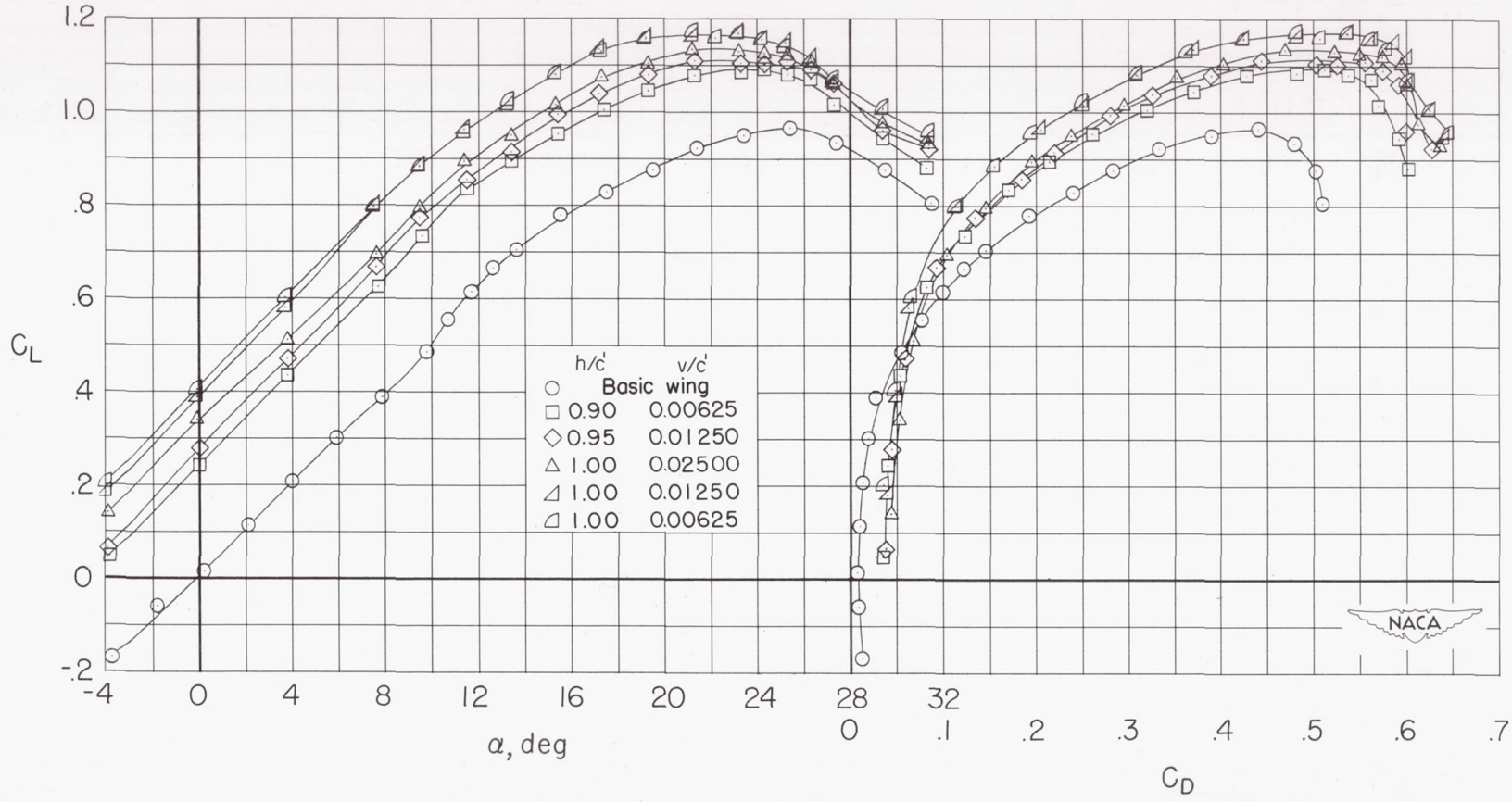

(a) C_L versus α. (b) C_L versus C_D.

Figure 7.- Effect of Fowler flap location on aerodynamic characteristics of the semispan 49.1° sweptback wing. $R \times 10^{-6} = 6.1$; $\delta_{ff} = 45°$; $\delta_{pf} = 0°$.

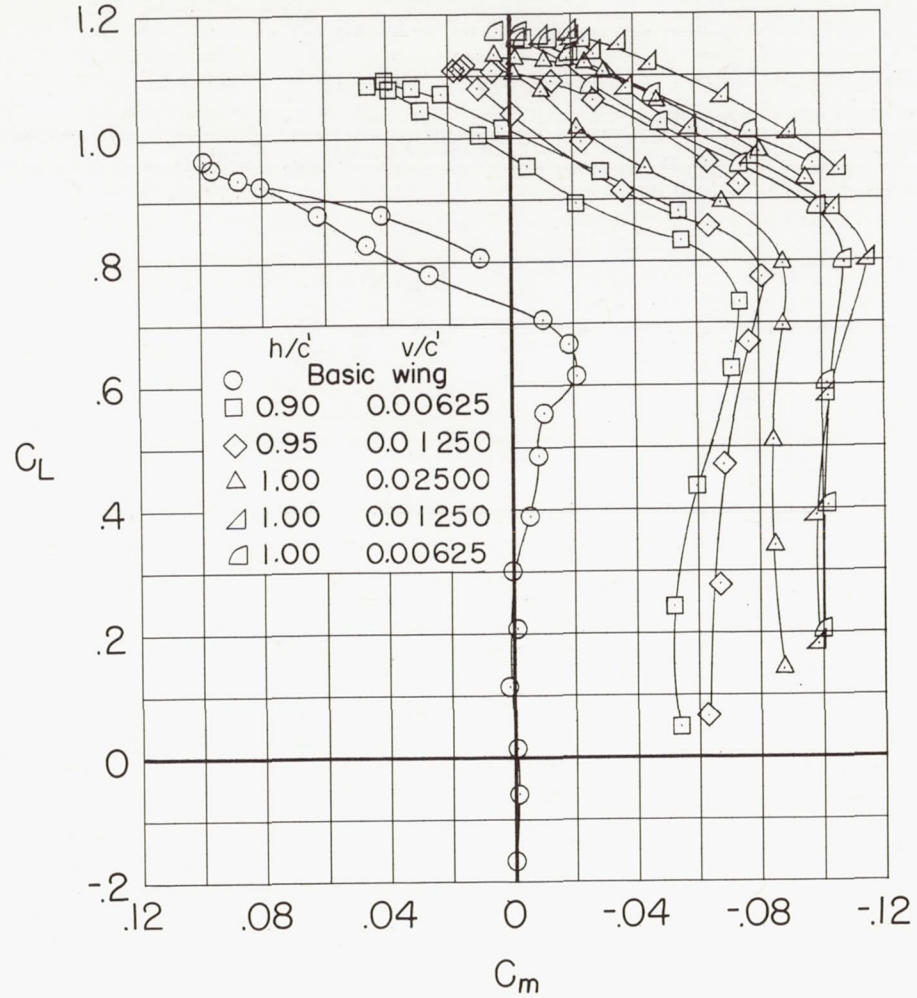

(c) C_L versus C_m.

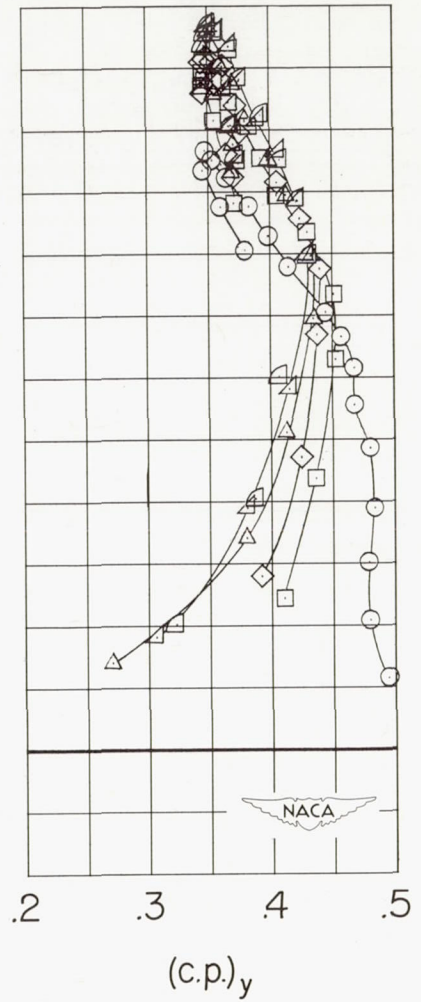

(d) C_L versus $(c.p.)_y$.

Figure 7.- Concluded.

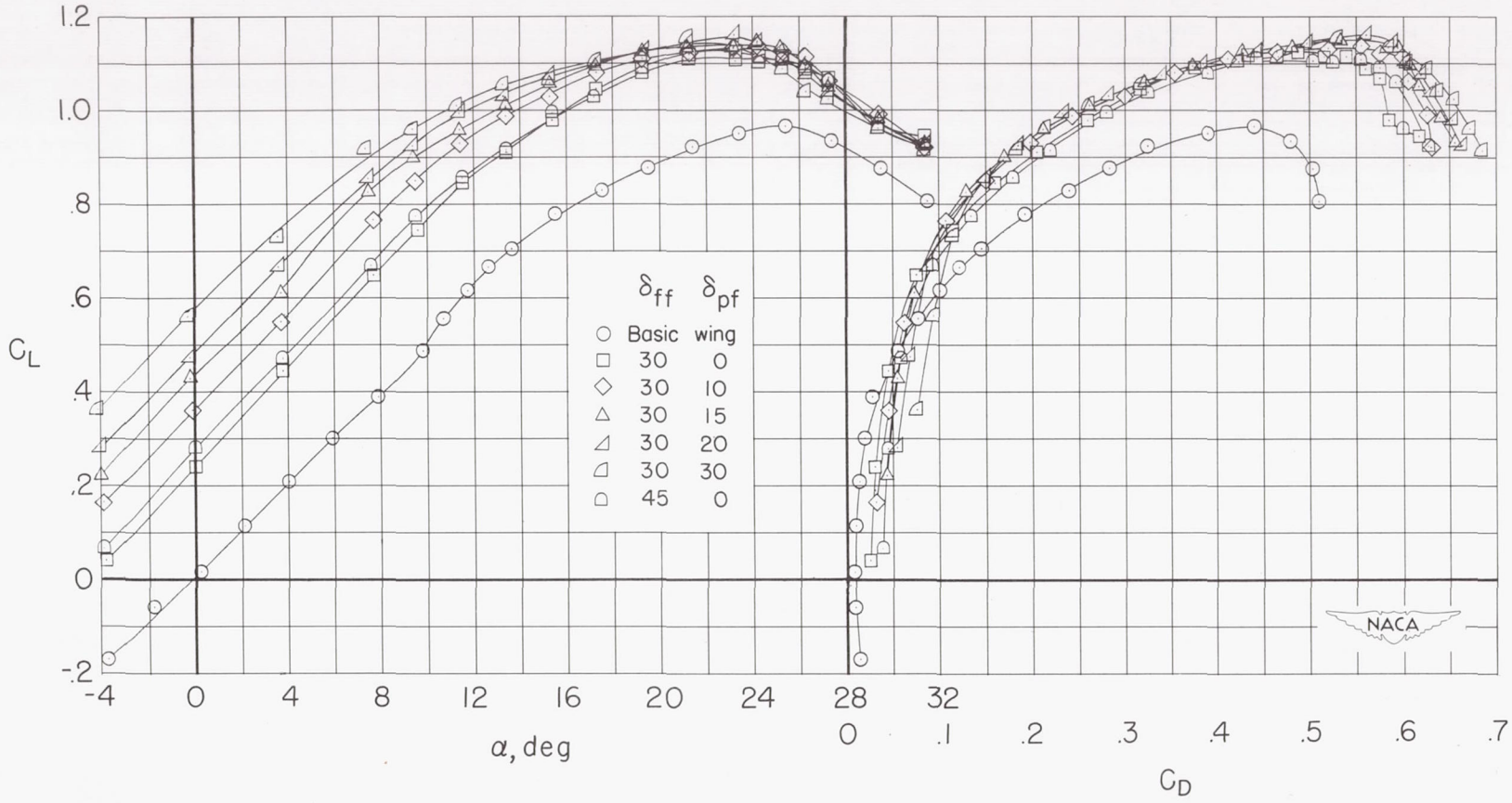

(a) C_L versus α. (b) C_L versus C_D.

Figure 8.- Effect of Fowler flap and plain-flap deflection on the aerodynamic characteristics of the semispan 49.1° sweptback wing. $R \times 10^{-6} = 6.1$; $h/c' = 0.95$; $v/c' = 0.01250$.

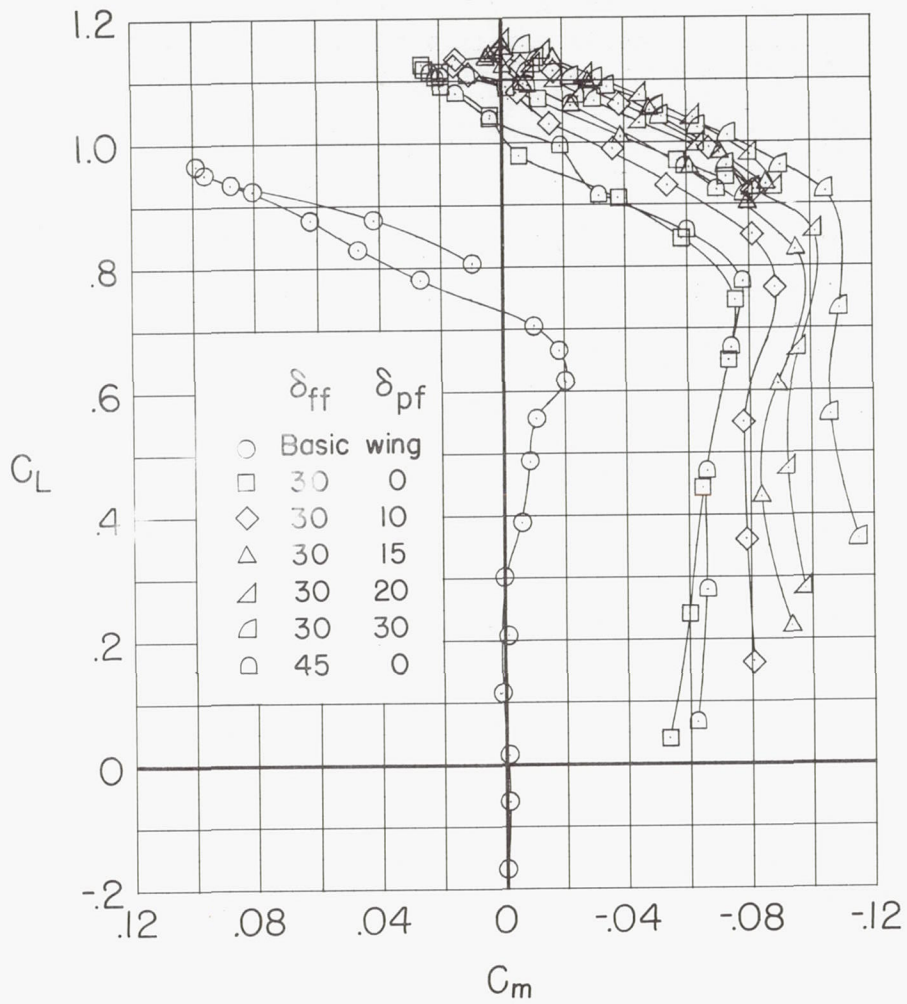

(c) C_L versus C_m.

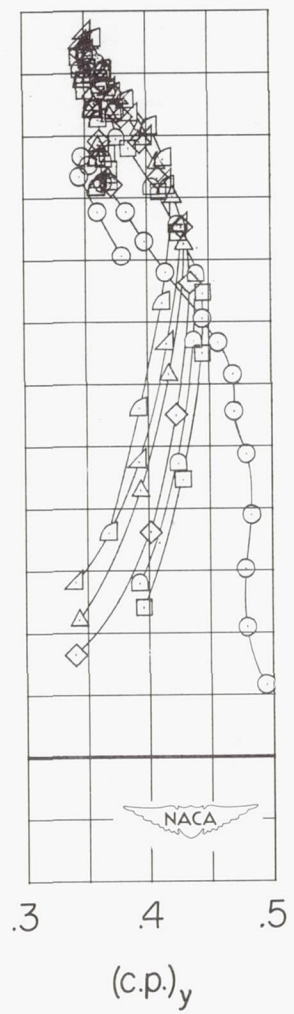

(d) C_L versus $(c.p.)_y$.

Figure 8.- Concluded.

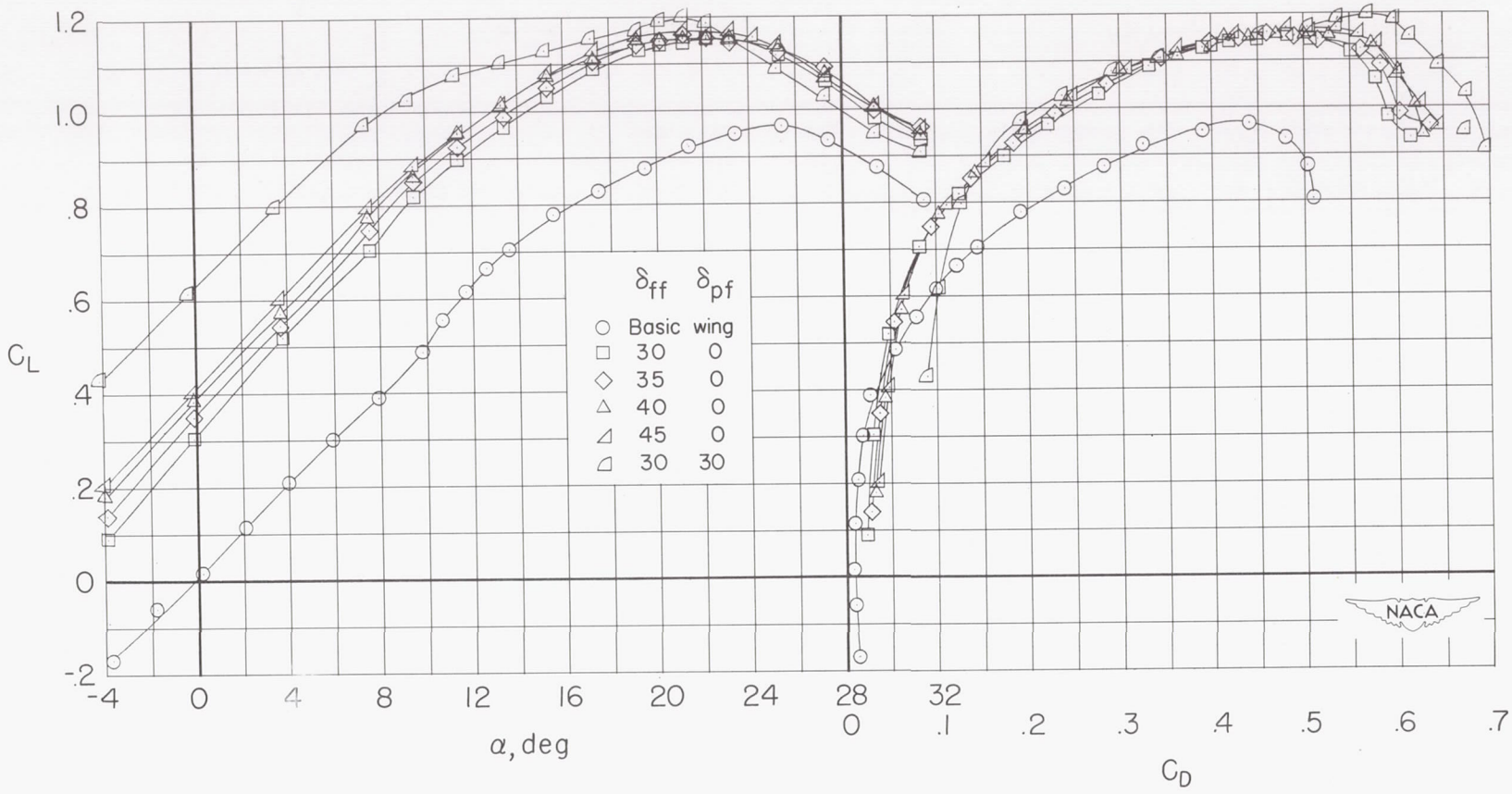

(a) C_L versus α. (b) C_L versus C_D.

Figure 9.- Effect of Fowler flap and plain-flap deflection on the aerodynamic characteristics of the semispan 49.1° sweptback wing. $R \times 10^{-6} = 6.1$; $h/c' = 1.00$; $v/c' = 0.00625$.

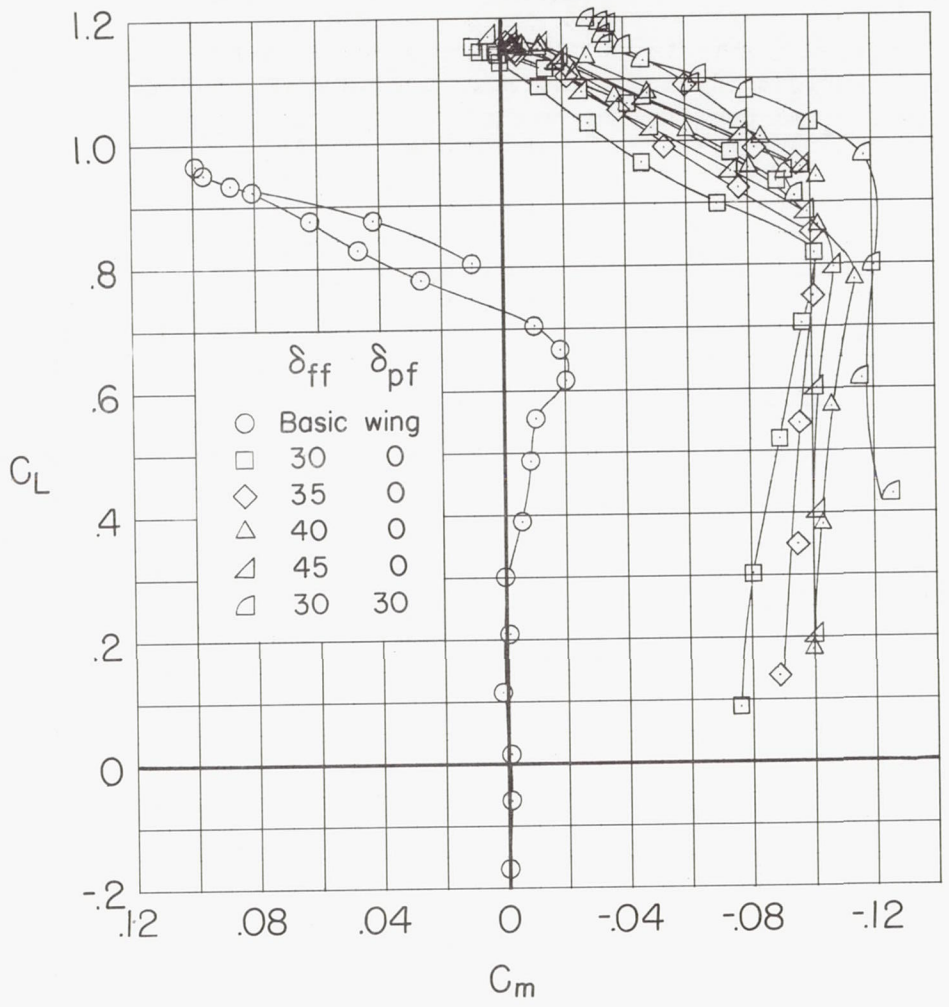

(c) C_L versus C_m.

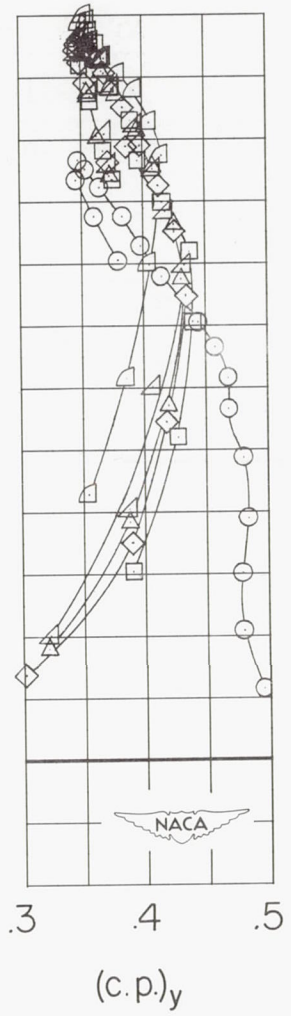

(d) C_L versus $(c.p.)_y$.

Figure 9.- Concluded.

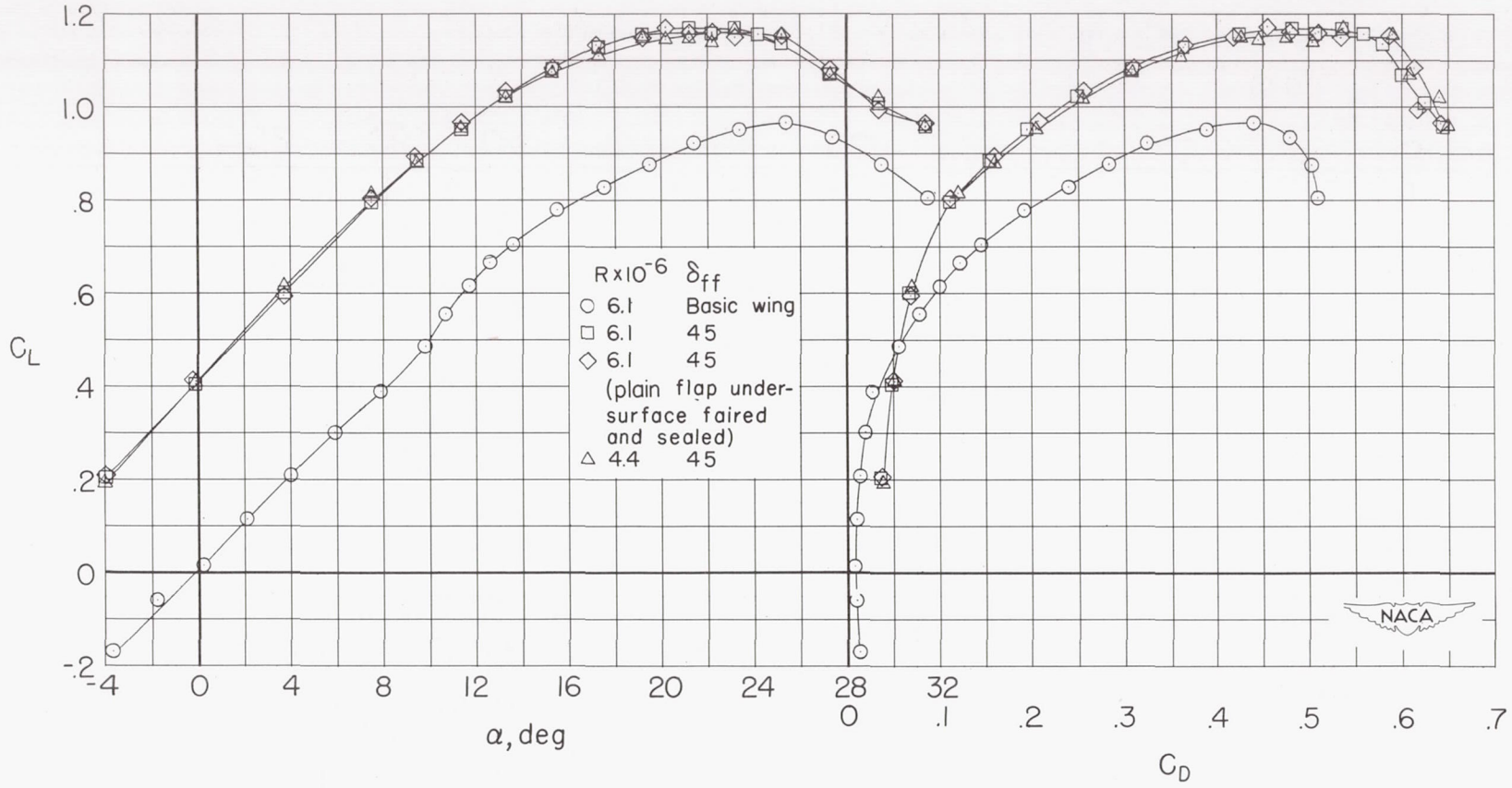

(a) C_L versus α. (b) C_L versus C_D.

Figure 10.- Effect of a Fowler flap, with and without the plain-flap undersurface faired and sealed, and Reynolds number on aerodynamic characteristics of the semispan 49.1° sweptback wing. h/c' = 1.00; v/c' = 0.00625; $\delta_{pf} = 0°$.

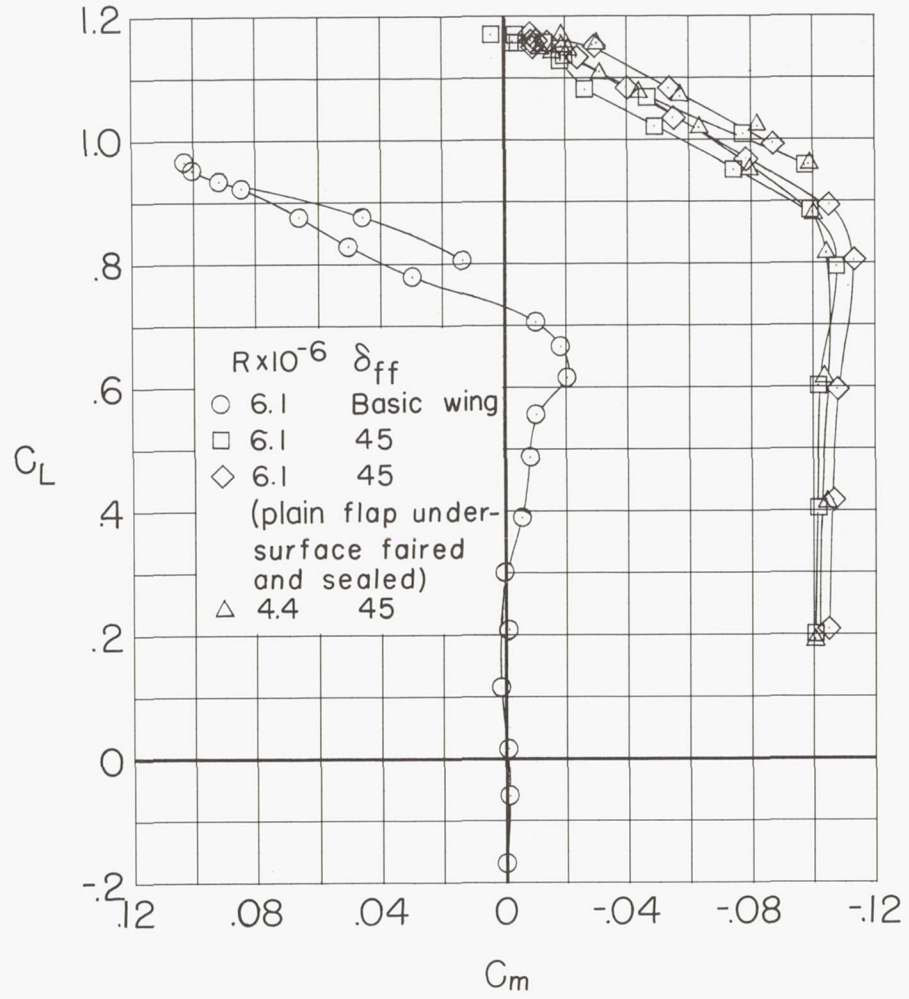

(c) C_L versus C_m.

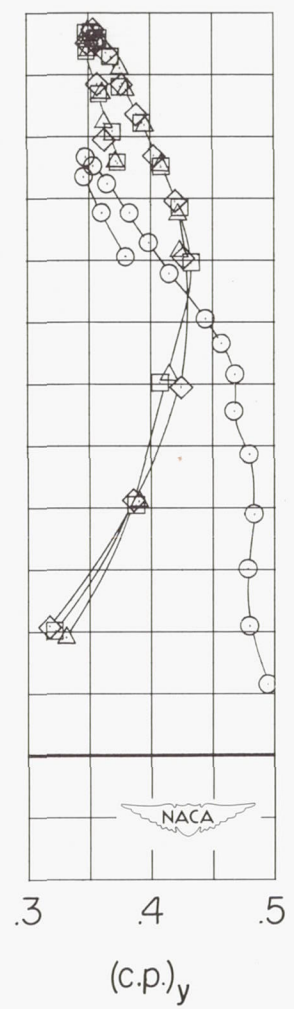

(d) C_L versus $(c.p.)_y$.

Figure 10.- Concluded.

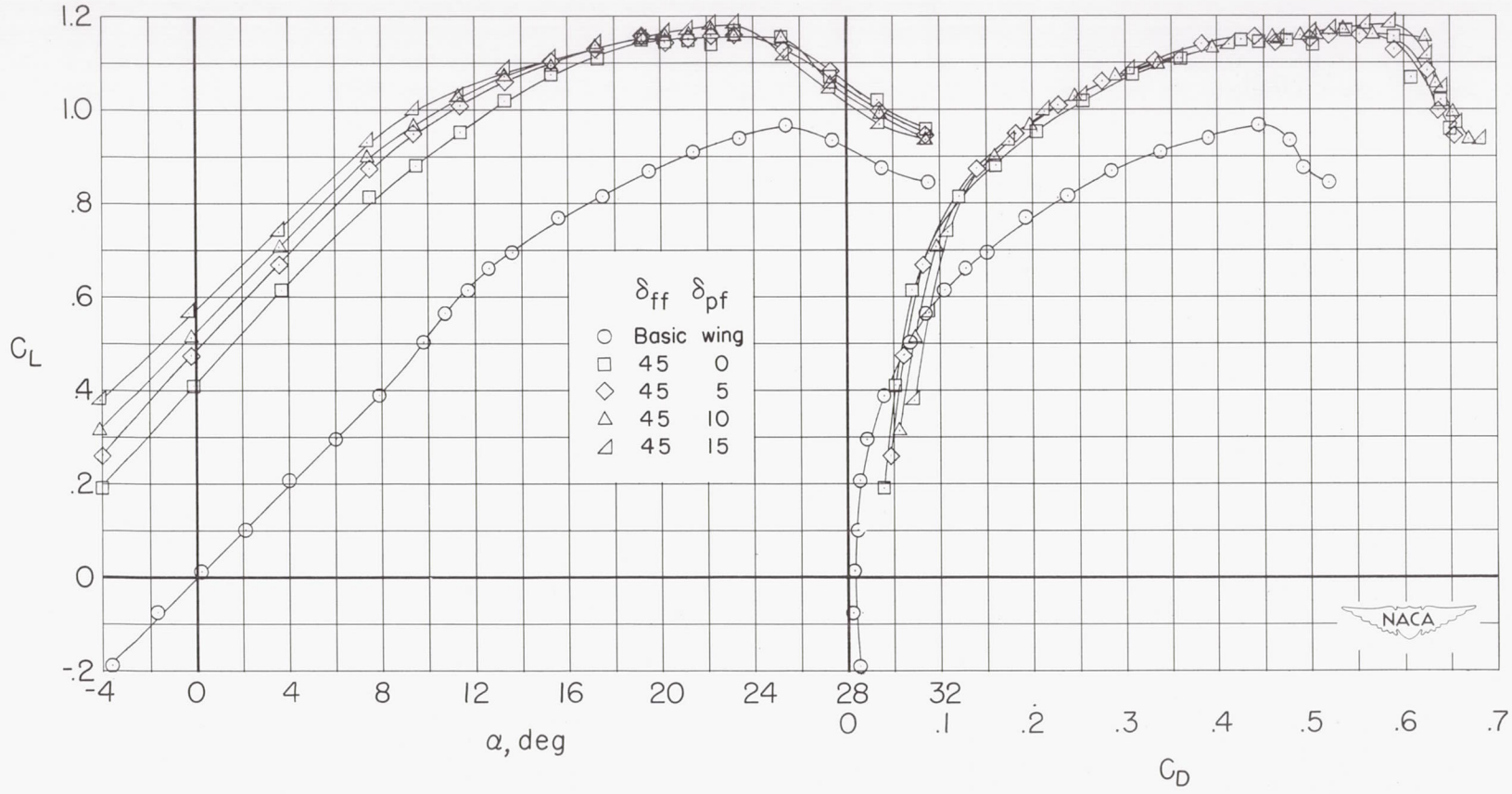

(a) C_L versus α. (b) C_L versus C_D.

Figure 11.- Effect of plain-flap deflection on aerodynamic characteristics of the semispan 49.1° sweptback wing. $R \times 10^{-6} = 4.4$; $h/c' = 1.00$; $v/c' = 0.00625$.

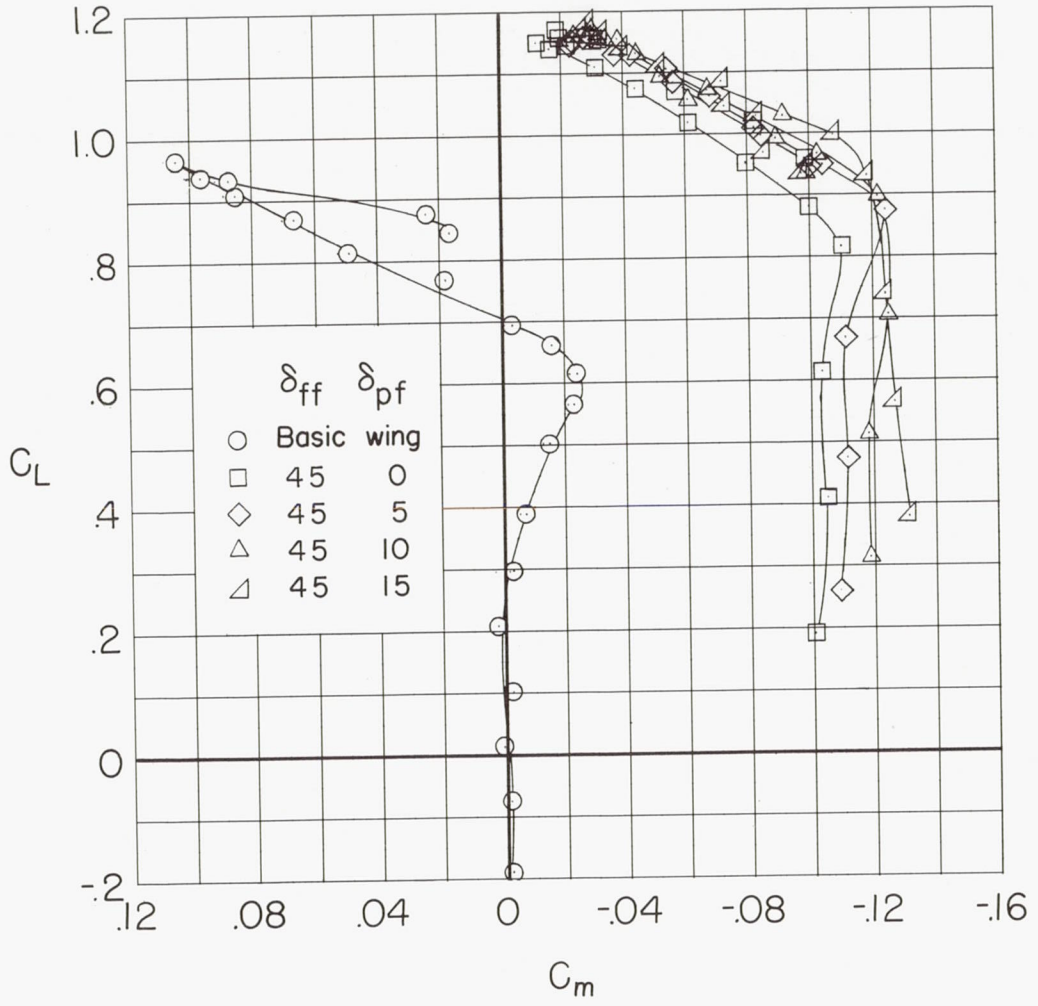

(c) C_L versus C_m.

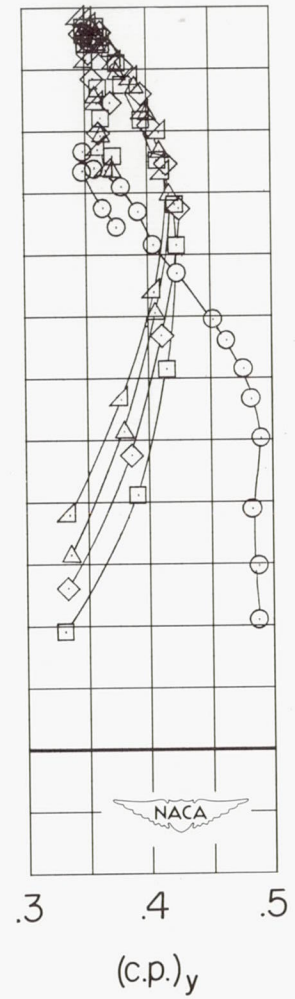

(d) C_L versus $(c.p.)_y$.

Figure 11.- Concluded.

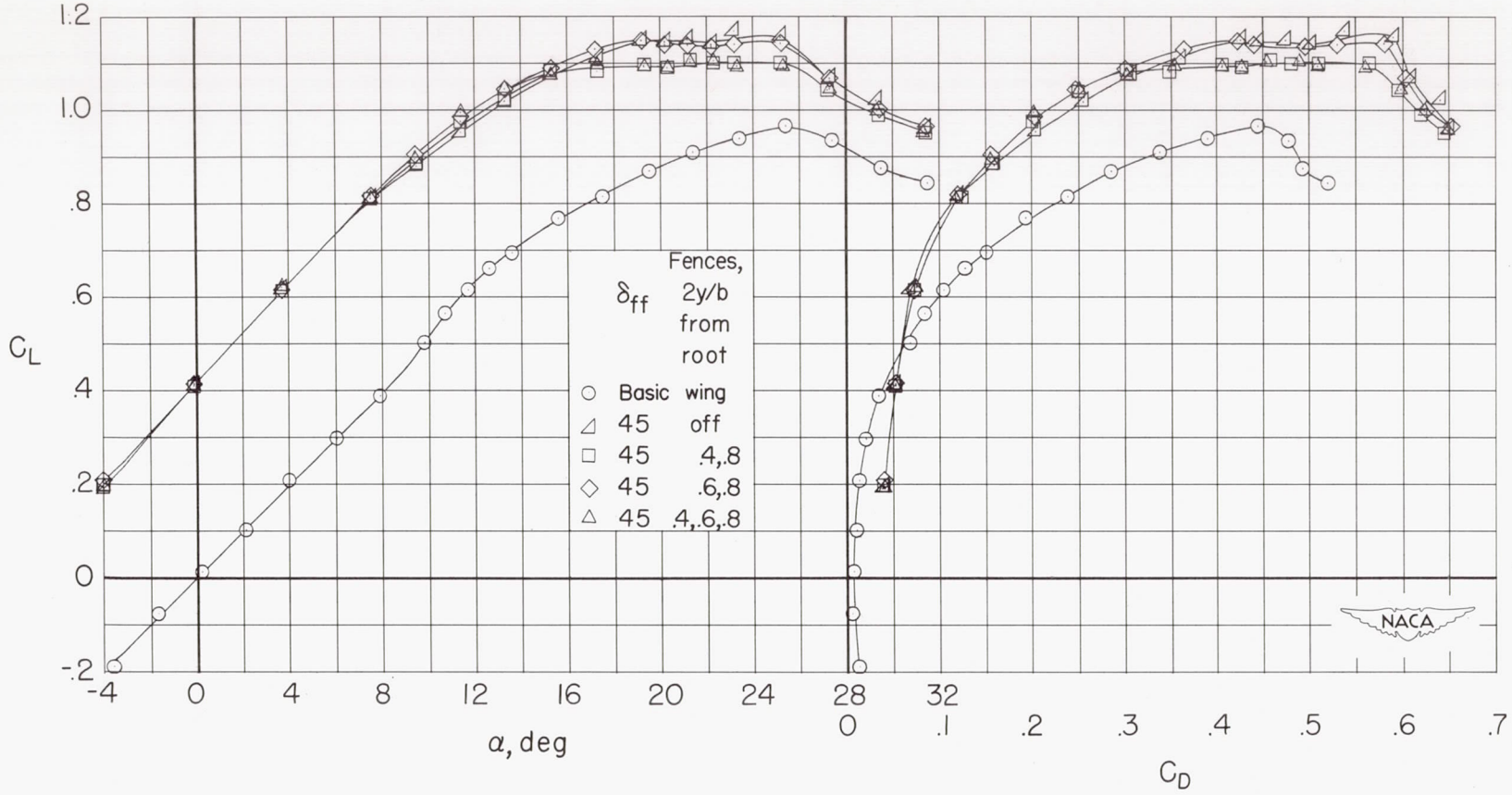

(a) C_L versus α. (b) C_L versus C_D.

Figure 12.- Effect of several full-chord fences on aerodynamic characteristics of the semispan 49.1° sweptback wing. $R \times 10^{-6} = 4.4$; $h/c' = 1.00$; $v/c' = 0.00625$; $\delta_{pf} = 0°$.

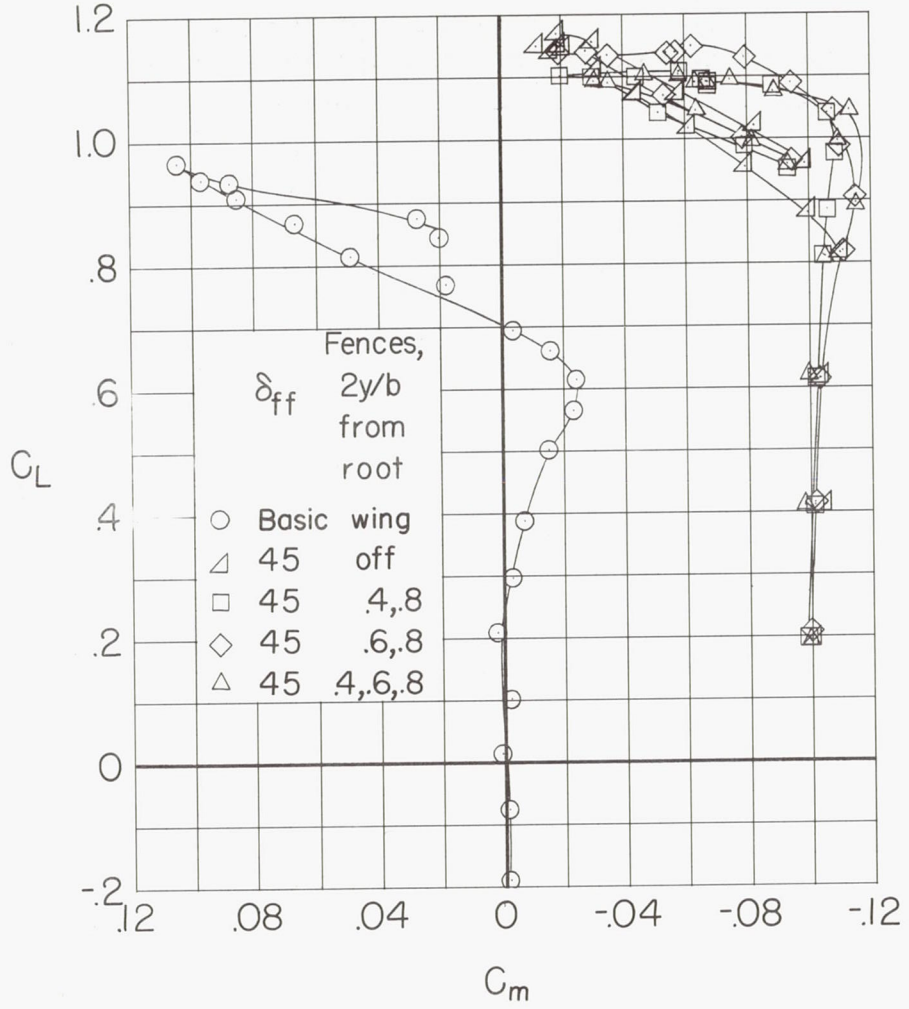

(c) C_L versus C_m.

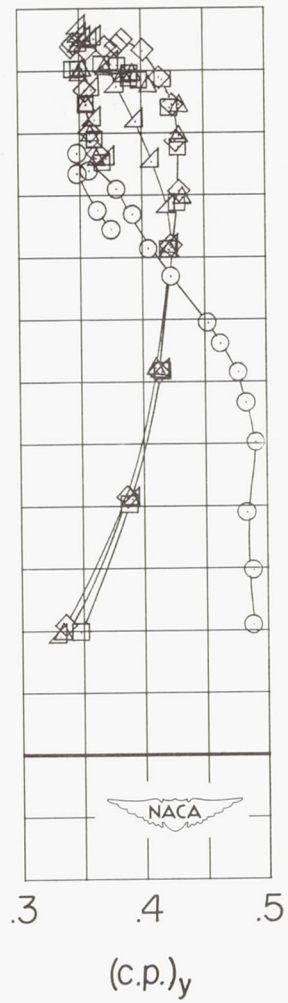

(d) C_L versus $(c.p.)_y$.

Figure 12.- Concluded.

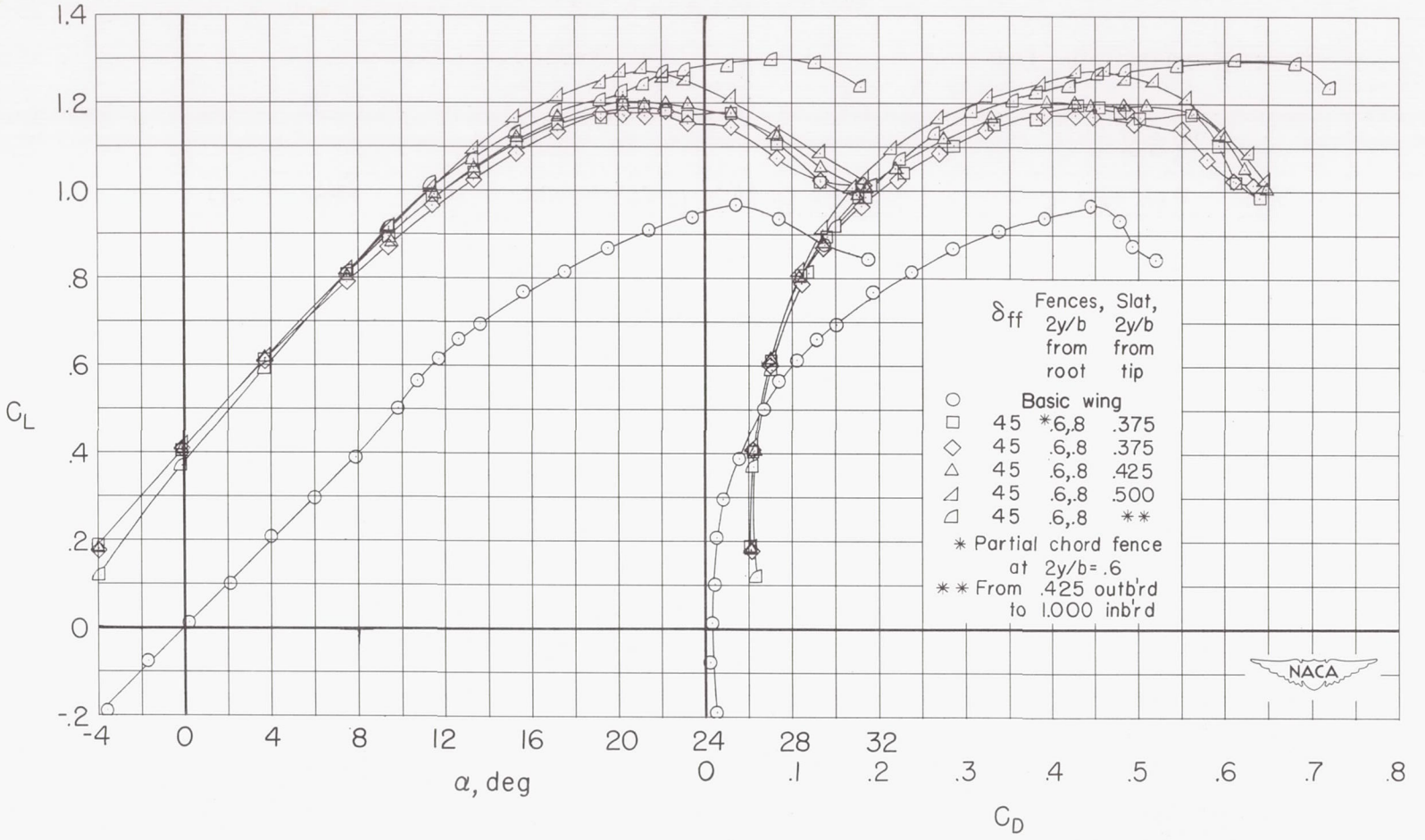

(a) C_L versus α. (b) C_L versus C_D.

Figure 13.- Effect of various fence and slat combinations on aerodynamic characteristics of the semispan 49.1° sweptback wing. $R \times 10^{-6} = 4.4$; $h/c' = 1.00$; $v/c' = 0.00625$; $\delta_{pf} = 0°$.

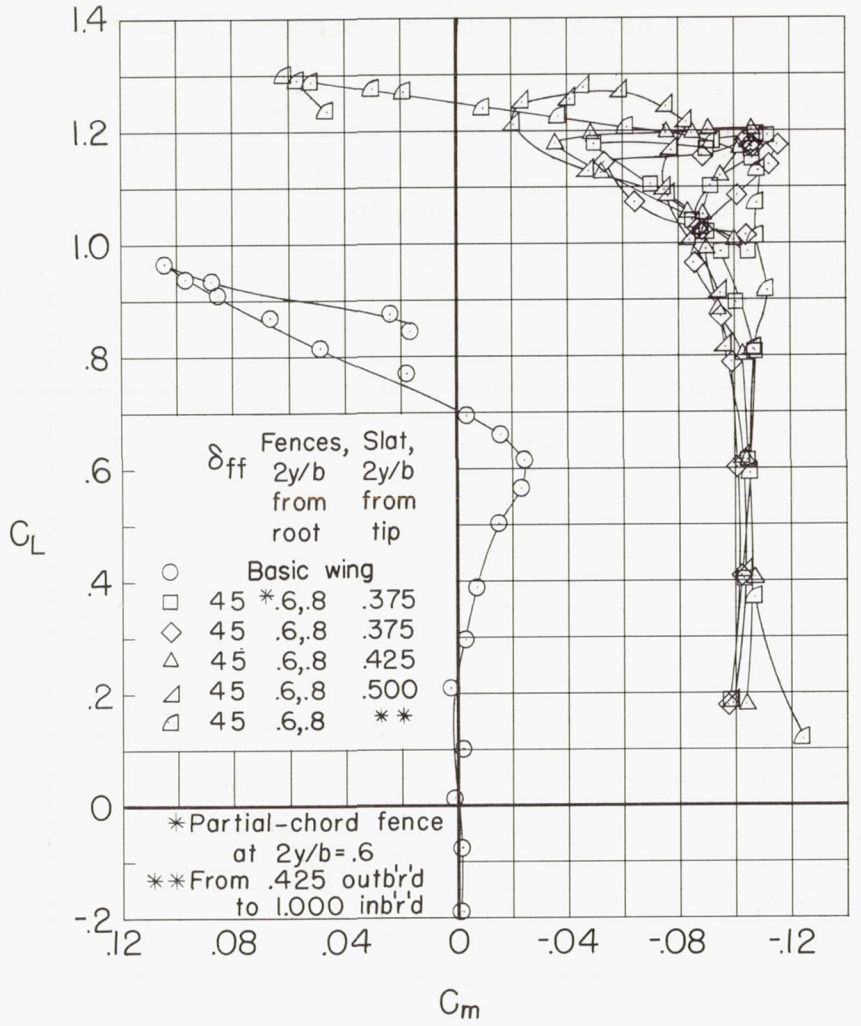

(c) C_L versus C_m.

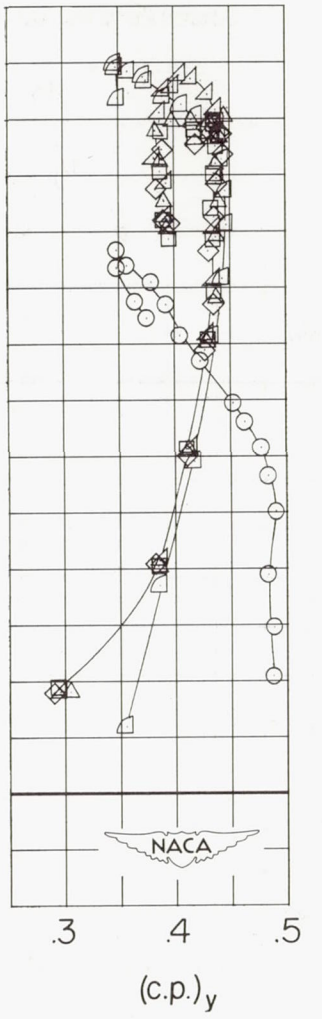

(d) C_L versus $(c.p.)_y$.

Figure 13.- Concluded.

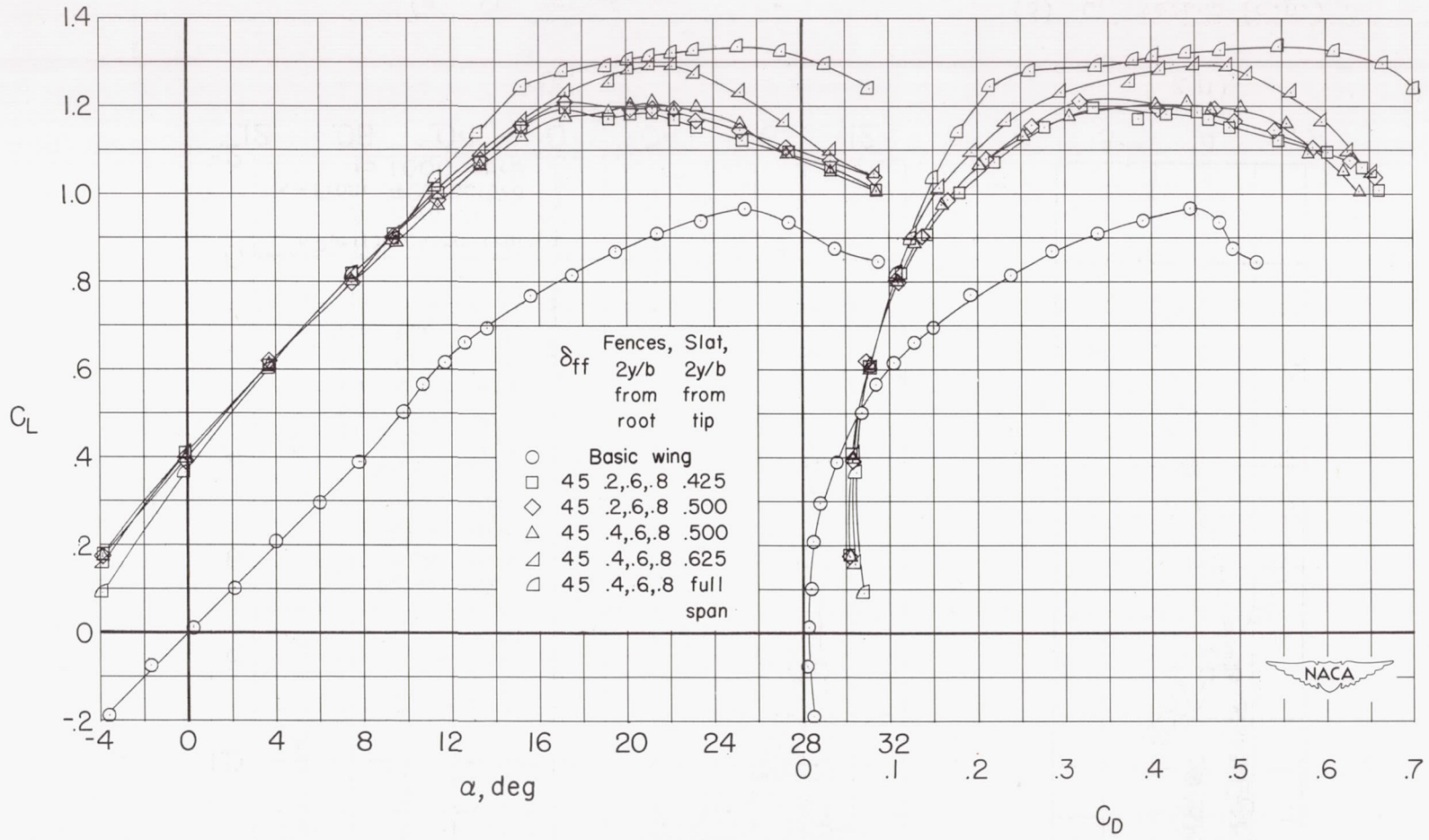

(a) C_L versus α. (b) C_L versus C_D.

Figure 14.- Effect of various fence and slat combinations on aerodynamic characteristics of the semispan 49.1° sweptback wing. $R \times 10^{-6} = 4.4$; $h/c' = 1.00$; $v/c' = 0.00625$; $\delta_{pf} = 0°$.

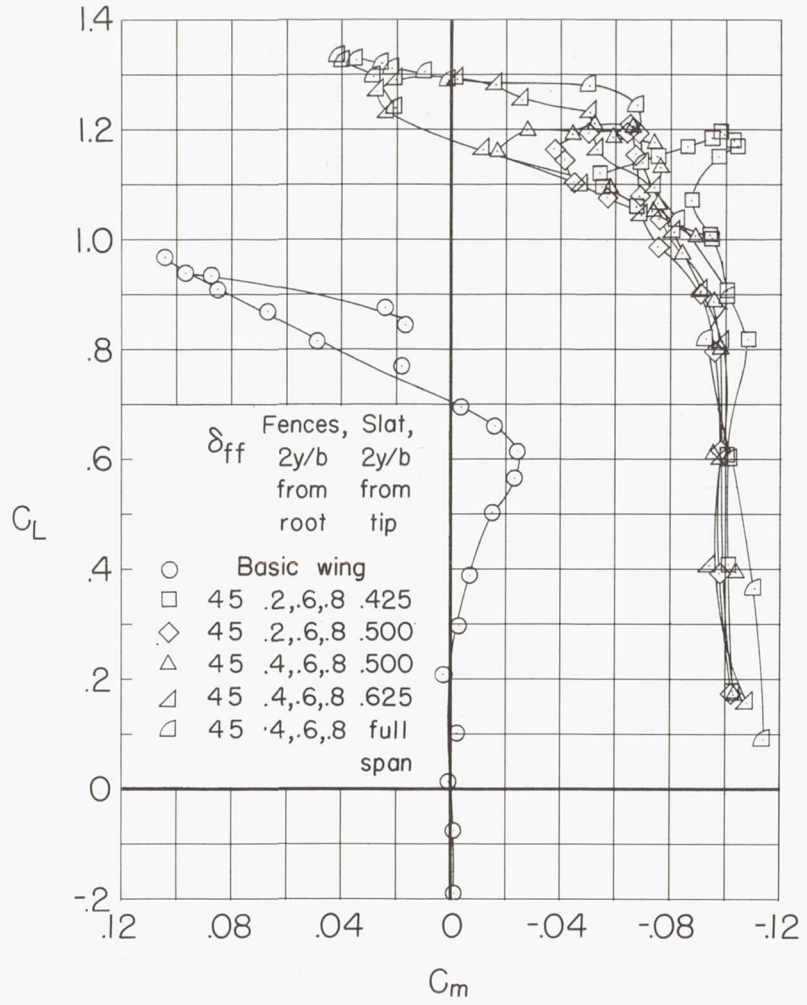

(c) C_L versus C_m.

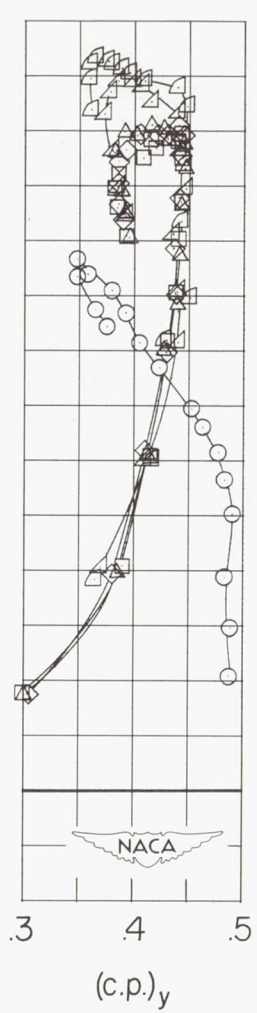

(d) C_L versus $(c.p.)_y$.

Figure 14.- Concluded.

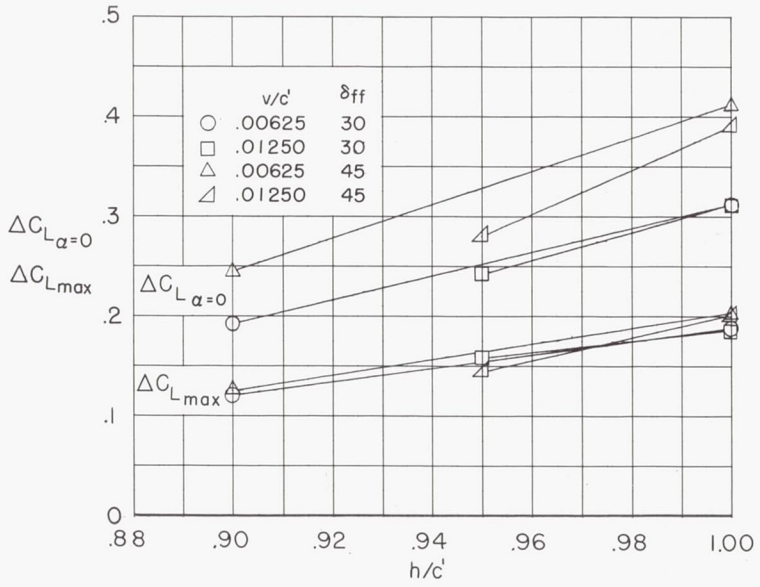

(a) Effect of chordwise hinge position.

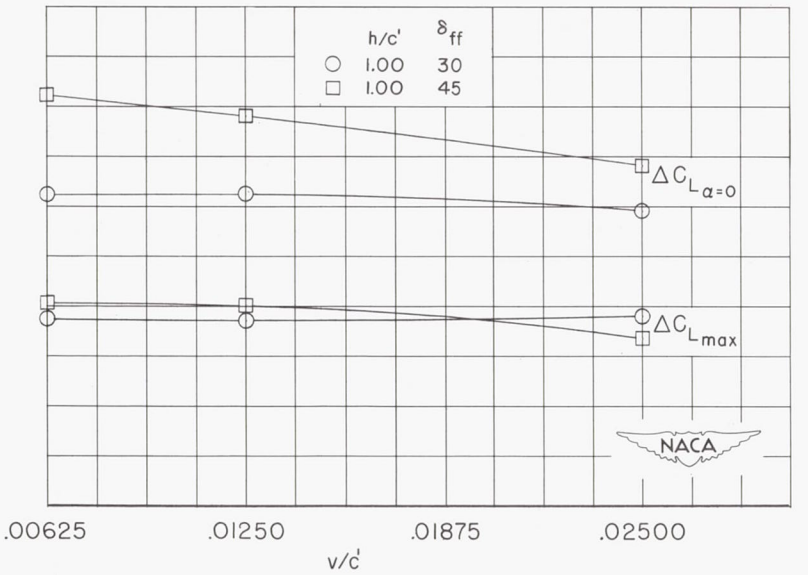

(b) Effect of gap size.

Figure 15.- Summary of the effect of Fowler flap hinge location for Fowler flap deflections of 30° and 45° on $\Delta C_{L_{max}}$ and $\Delta C_{L_{\alpha=0}}$. $R \times 10^{-6} = 6.1$; $\delta_{pf} = 0°$.

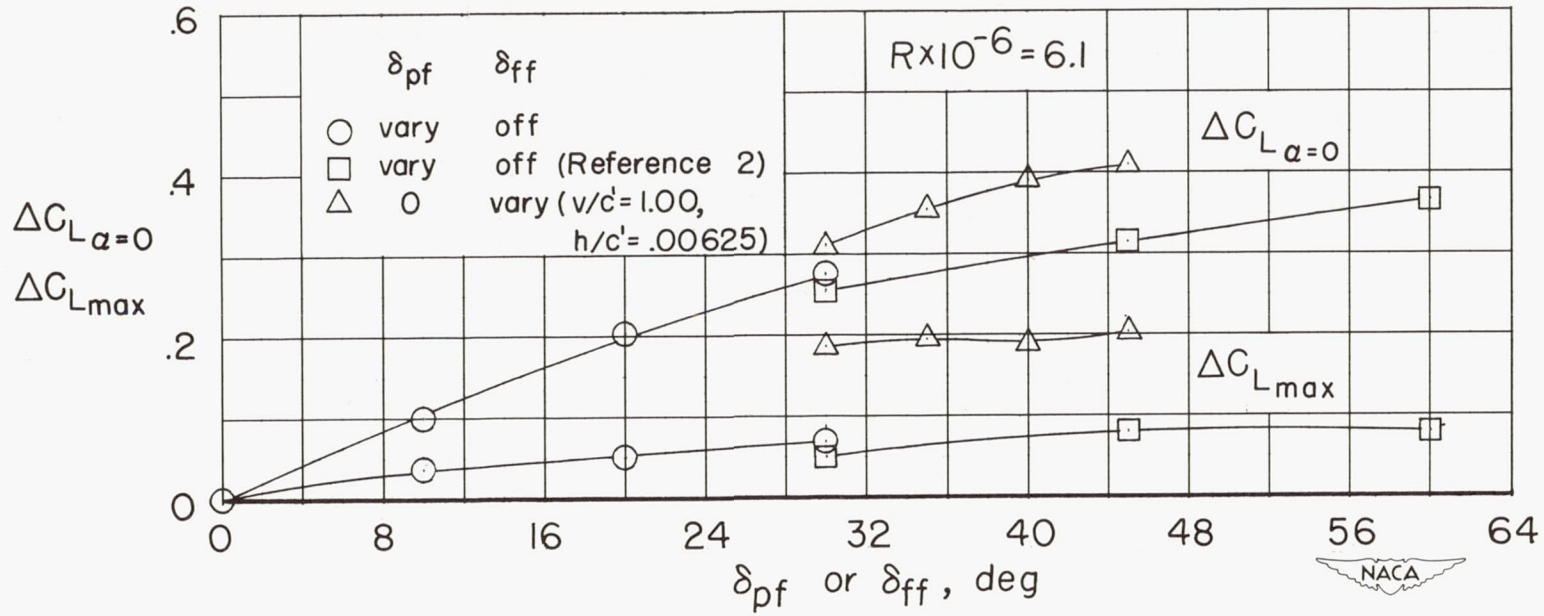

Figure 16.- Summary of the effect of Fowler flap and plain-flap deflection on $\Delta C_{L_{max}}$ and $\Delta C_{L_{\alpha=0}}$.

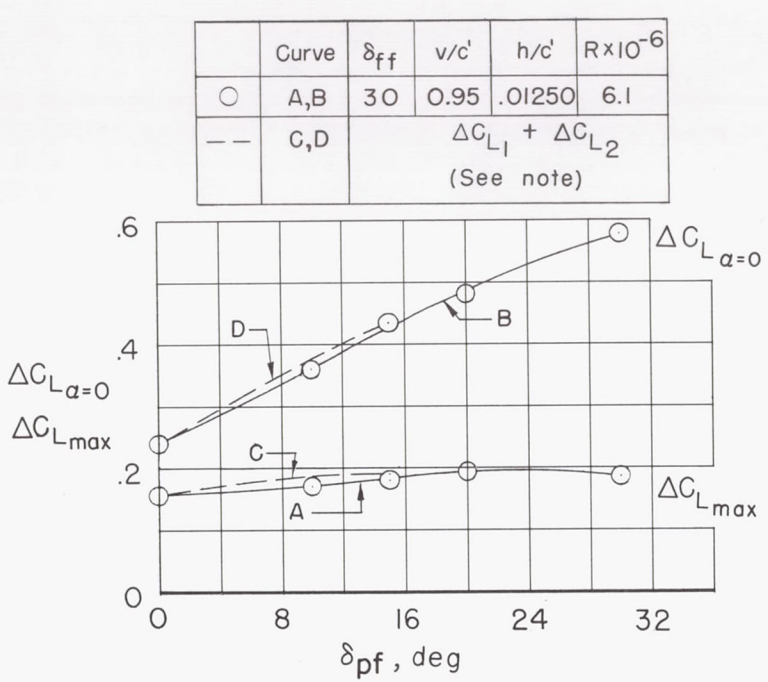

Note: $\Delta C_{L_1} = \Delta C_L$ for δ_{ff} at v/c'= 0.95, h/c'= .01250, δ_{pf} = 0 (figure 15(a))

$\Delta C_{L_2} = \Delta C_L$ for δ_{pf}, Fowler flap off (figure 16)

(a) Comparison of predicted and experimental results for $\delta_{ff} = 30^\circ$.

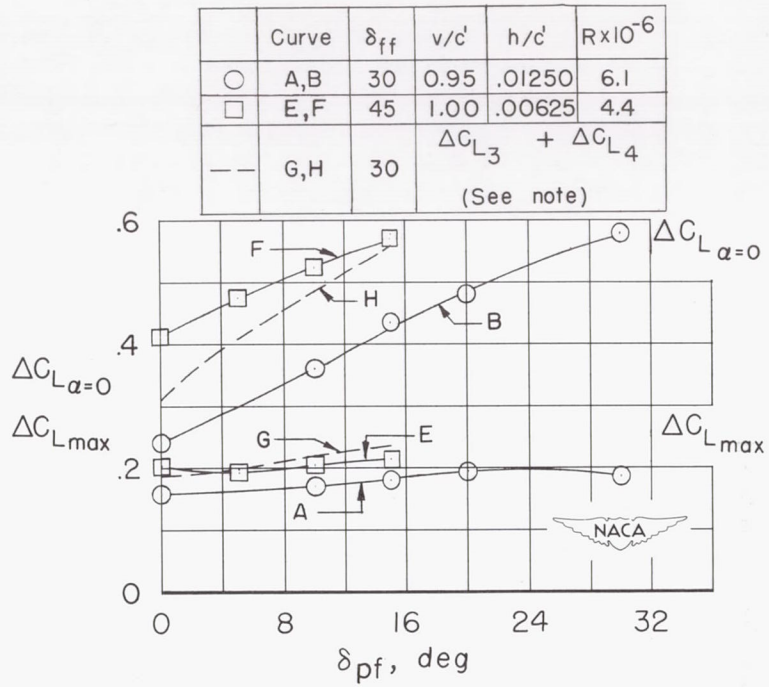

Note: $\Delta C_{L_3} = \Delta C_L$ for δ_{ff} at v/c'= 1.00, h/c'= .00625, δ_{pf} = 0 (figure 16)

$\Delta C_{L_4} = \Delta C_L$ for δ_{pf}, Fowler flap off (figure 16)

(b) Effect of Fowler flap deflection.

Figure 17.- Effect of the plain-flap deflection on the lift-coefficient increments due to the combination of plain flap and Fowler flap.

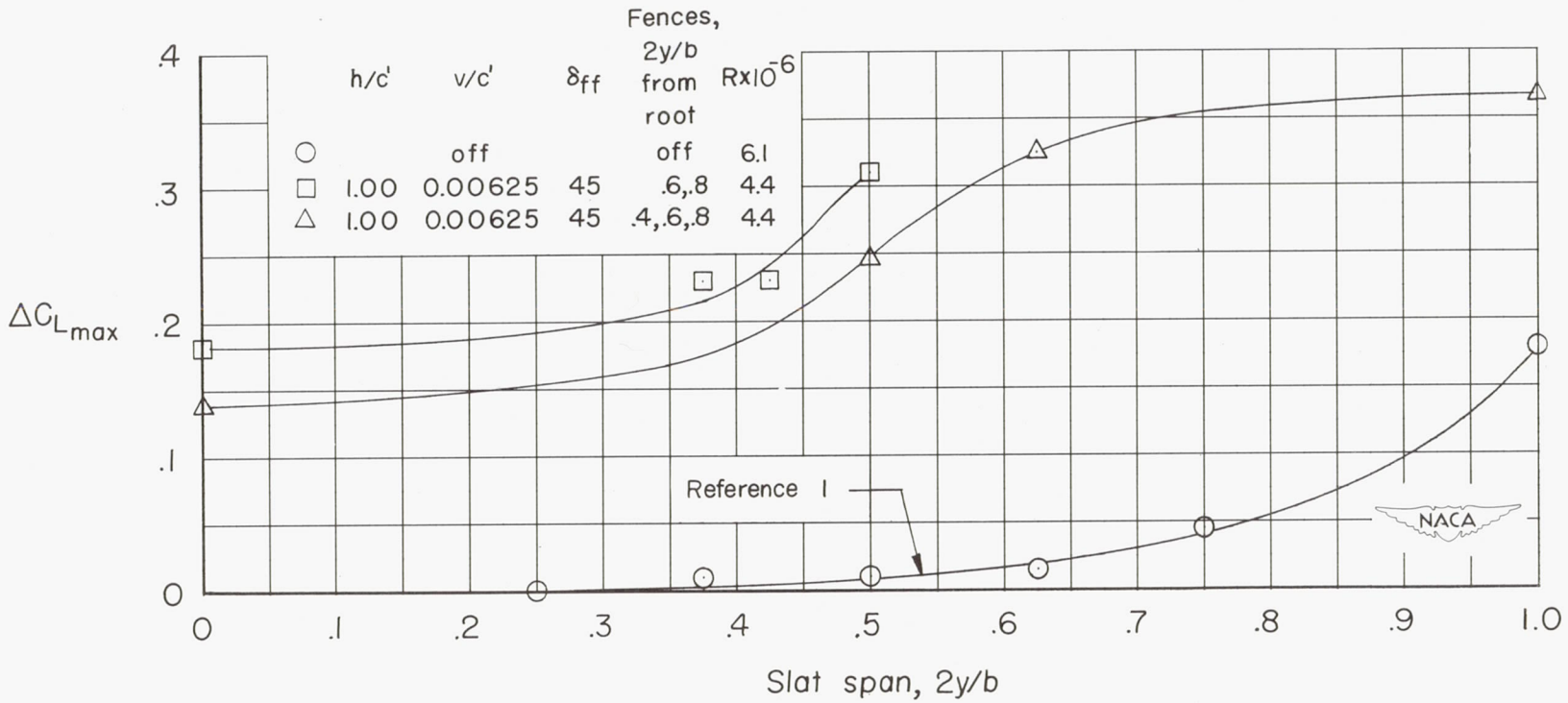

Figure 18.- Summary of the effect on $\Delta C_{L_{max}}$ of slat span.

NACA-Langley - 6-5-53 - 325